NATIONAL AND KAPODISTRIAN UNIVERSITY OF ATHENS

SCHOOL OF SCIENCE
DEPARTMENT OF INFORMATICS AND TELECOMMUNICATION

INTERDISCIPLINARY POSTGRADUATE PROGRAM
"INFORMATION TECHNOLOGIES IN MEDICINE AND BIOLOGY"

MASTER THESIS

A web-based crystallographic tool for the construction of nanoparticles

Alexios T. Chatzigoulas

Supervisor: **Dr. Zoe Cournia**, Researcher - Assistant Professor Level, Biomedical Research Foundation of the Academy of Athens (BRFAA)

ATHENS

FEBRUARY 2018

ΕΘΝΙΚΟ ΚΑΙ ΚΑΠΟΔΙΣΤΡΙΑΚΟ ΠΑΝΕΠΙΣΤΗΜΙΟ ΑΘΗΝΩΝ

ΣΧΟΛΗ ΘΕΤΙΚΩΝ ΕΠΙΣΤΗΜΩΝ
ΤΜΗΜΑ ΠΛΗΡΟΦΟΡΙΚΗΣ ΚΑΙ ΤΗΛΕΠΙΚΟΙΝΩΝΙΩΝ

ΔΙΑΤΜΗΜΑΤΙΚΟ ΜΕΤΑΠΤΥΧΙΑΚΟ ΠΡΟΓΡΑΜΜΑ
"ΤΕΧΝΟΛΟΓΙΕΣ ΠΛΗΡΟΦΟΡΙΚΗΣ ΣΤΗΝ ΙΑΤΡΙΚΗ ΚΑΙ ΤΗ ΒΙΟΛΟΓΙΑ"

ΔΙΠΛΩΜΑΤΙΚΗ ΕΡΓΑΣΙΑ

Ένα διαδικτυακό κρυσταλλογραφικό εργαλείο για την καταστευή νανοσωματιδίων

Αλέξιος Θ. Χατζηγούλας

Επιβλέπουσα: **Δρ. Ζωή Κούρνια**, Ερευνήτρια Γ', Ίδρυμα Ιατροβιολογικών Ερευνών Ακαδημίας Αθηνών (ΙΙΒΕΑΑ)

ΑΘΗΝΑ

ΦΕΒΡΟΥΑΡΙΟΣ 2018

MASTER THESIS

A web-based crystallographic tool for the construction of nanoparticles

Alexios T. Chatzigoulas
S.N.: PIV0155

SUPERVISOR: **Dr. Zoe Cournia**, Researcher - Assistant Professor Level, Biomedical Research Foundation of the Academy of Athens (BRFAA)

EXAMINATION COMMITTEE: **Dr. Zoe Cournia,** Researcher - Assistant Professor Level, Biomedical Research Foundation of the Academy of Athens (BRFAA)
Dr. Ioannis Emiris, Professor Level, National and Kapodistrian University of Athens (NKUA), Department of Informatics and Telecommunications (DIT)
Dr. Evangelia Chrysina, Senior Researcher at the Institute of Biology, Medicinal Chemistry and Biotechnology, National Hellenic Research Foundation (NHRF) and Associate Professor at Orebro University, Sweden

FEBRUARY 2018

ΔΙΠΛΩΜΑΤΙΚΗ ΕΡΓΑΣΙΑ

Ένα διαδικτυακό κρυσταλλογραφικό εργαλείο για την καταστευή νανοσωματιδίων

Αλέξιος Θ. Χατζηγούλας
Α.Μ.: ΤΠΙΒ0155

ΕΠΙΒΛΕΠΟΥΣΑ: **Δρ. Ζωή Κούρνια,** Ερευνήτρια Γ', Ίδρυμα Ιατροβιολογικών Ερευνών Ακαδημίας Αθηνών (ΙΙΒΕΑΑ)

ΕΞΕΤΑΣΤΙΚΗ ΕΠΙΤΡΟΠΗ: **Δρ. Ζωή Κούρνια**, Ερευνήτρια Γ', Ίδρυμα Ιατροβιολογικών Ερευνών Ακαδημίας Αθηνών (ΙΙΒΕΑΑ)
Δρ. Ιωάννης Εμίρης, Καθηγητής, Εθνικό και Καποδιστριακό Πανεπιστήμιο Αθηνών (ΕΚΠΑ), Τμήμα Πληροφορικής και Τηλεπικοινωνιών (ΤΠΛ)
Δρ. Ευαγγελία Χρυσίνα, Ερευνήτρια Β' Ινστιτούτο Βιολογίας, Φαρμακευτικής Χημείας και Βιοτεχνολογίας, Εθνικό Ίδρυμα Ερευνών & Αναπληρώτρια Καθηγήτρια στο Πανεπιστήμιο του Orebro, Σουηδία

ΦΕΒΡΟΥΑΡΙΟΣ 2018

ABSTRACT

Nanoparticles have various applications in medicine, physics, optics, and electronics. Modeling nanoparticles is an essential first step to assess their capacity in different uses such as in energy storage or drug delivery. However, creating an initial starting conformation for modeling and simulation is tedious, because every crystalline material grows with a different crystal habit and different symmetry in nature.

In this diploma thesis, a web-based crystallographic tool has been created, which creates nanoparticle models from any crystal structure guided by their preferred equilibrium shape in standard conditions according to Wulff morphology (crystal habit).

The algorithm uses input from quantum mechanical calculations based on the Wulff construction. The Wulff construction employs energy minimization arguments to demonstrate that specific crystal planes are preferred over others, with their distance from the origin being proportional to their surface energy. The input parameters for determining this equilibrium nanoparticle structure are the preferred growing planes as Miller indices, the energy of each plane, and the desired size of the nanoparticle.

After inputting this data, the equilibrium shape is created with the following methodology. First, based on the crystallographic point group, the symmetric planes are produced based on the Miller indices, the fractional coordination system, and the lattice parameters. In this procedure, we place the origin on the negative side of these planes, and then we calculate the intersection points per three of the planes, discarding those that are on the positive side of at least one of the planes. Then, we obtain the faces of the equilibrium shape using the Quickhull algorithm on the remaining intersection points, and the equilibrium shape is constructed by connecting these faces. The symmetric unit cell of the crystal structure is produced from the asymmetric one, using the lattice parameters and the symmetry operations of the crystallographic space group on the coordinates of the atoms again. Finally, the nanoparticle is constructed by replication of the unit cell across all three spatial directions, until the equilibrium shape is filled, and the coordinates of the atoms are output to the user.

This tool may be used to construct nanoparticles for simulation of any material given the crystal structure as input, the size of the nanoparticle, and the preferred growing planes and energies. It has been implemented as a website using C++ and PHP and can be accessed and used at http://nanocrystal.vi-seem.eu/CrystalTool.

ΠΕΡΙΛΗΨΗ

Τα νανοσωματίδια έχουν διάφορες εφαρμογές στην ιατρική, τη φυσική, την οπτική και την ηλεκτρονική. Η μοντελοποίηση νανοσωματιδίων είναι ένα ουσιαστικό πρώτο βήμα για να εκτιμηθεί η ικανότητα τους σε διάφορες χρήσεις όπως η αποθήκευση ενέργειας ή η μεταφορά φαρμάκων. Ωστόσο, η δημιουργία μιας αρχικής σύνθεσης για μοντελοποίηση και προσομοίωση είναι κουραστική, επειδή κάθε κρύσταλλος αναπτύσσεται με διαφορετικό crystal habit και διαφορετική συμμετρία στη φύση.

Σε αυτή τη διπλωματική εργασία, δημιουργήθηκε ένα διαδικτυακό κρυσταλλογραφικό εργαλείο, το οποίο δημιουργεί μοντέλα νανοσωματιδίων από οποιαδήποτε κρυσταλλική δομή σύμφωνα με το προτιμώμενο σχήμα ισορροπίας τους σε τυπικές συνθήκες σύμφωνα με τη μορφολογία Wulff (crystal habit).

Ο αλγόριθμος χρησιμοποιεί δεδομένα από κβαντομηχανικούς υπολογισμούς βάσει της κατασκευής Wulff. Η κατασκευή Wulff χρησιμοποιεί παραμέτρους ελαχιστοποίησης της ενέργειας για να καταδείξει ότι ορισμένες έδρες προτιμώνται σε σχέση με άλλες, καθώς η απόστασή τους από το κέντρο είναι ανάλογη με την ενέργεια της επιφάνειας τους. Οι παράμετροι εισόδου για τον προσδιορισμό αυτής της δομής νανοσωματιδίων σε ισορροπία είναι οι έδρες που προτιμώνται να αναπτύσσονται, ως δείκτες Miller, η ενέργεια κάθε επιπέδου και το επιθυμητό μέγεθος του νανοσωματιδίου.

Μετά την εισαγωγή αυτών των παραμέτρων, το σχήμα ισορροπίας δημιουργείται με την ακόλουθη μεθοδολογία. Πρώτον, με βάση την κρυσταλλογραφική τάξη, οι συμμετρικές έδρες παράγονται με βάση τους δείκτες Miller, το κλασματικό σύστημα συντεταγμένων και τις παραμέτρους του κρυσταλλικού πλέγματος. Σε αυτή τη διαδικασία, τοποθετούμε την αρχή των αξόνων στην αρνητική πλευρά αυτών των εδρών και στη συνέχεια υπολογίζουμε τα σημεία τομής ανά τρις έδρες, απορρίπτοντας αυτά που βρίσκονται στη θετική πλευρά τουλάχιστον ενός εκ των εδρών. Στη συνέχεια, λαμβάνουμε τις όψεις του σχήματος ισορροπίας χρησιμοποιώντας τον αλγόριθμο Quickhull στα εναπομείναντα σημεία τομής και το σχήμα ισορροπίας κατασκευάζεται συνδέοντας αυτές τις όψεις. Η στοιχειώδης κυψελίδα της κρυσταλλικής δομής παράγεται από την ασύμμετρη κυψελίδα, χρησιμοποιώντας πάλι τις παραμέτρους του κρυσταλλικού πλέγματος και τις λειτουργίες συμμετρίας της κρυσταλλογραφικής χωρο-ομάδας στις συντεταγμένες των ατόμων. Τέλος, το νανοσωματίδιο κατασκευάζεται με την αντιγραφή της στοιχειώδης κυψελίδας και στις τρεις χωρικές διευθύνσεις, μέχρις ότου γεμίσει το σχήμα ισορροπίας με αποτέλεσμα οι συντεταγμένες των ατόμων να εξάγονται στον χρήστη.

Αυτό το εργαλείο μπορεί να χρησιμοποιηθεί για την κατασκευή νανοσωματιδίων για προσομοίωση οποιουδήποτε υλικού, δεδομένης της κρυσταλλικής δομής ως είσοδο, του μεγέθους του νανοσωματιδίου και των προτιμώμενων εδρών ανάπτυξης και των ενεργειών τους. Έχει κατασκευαστεί ως διαδικτυακή σελίδα χρησιμοποιώντας τις προγραμματιστικές γλώσσες C++ και PHP και μπορεί να προσπελαστεί και να χρησιμοποιηθεί στην ιστοσελίδα http://nanocrystal.vi-seem.eu/CrystalTool.

ΘΕΜΑΤΙΚΗ ΠΕΡΙΟΧΗ: Φυσική Συμπυκνωμένης Ύλης

ΛΕΞΕΙΣ ΚΛΕΙΔΙΑ: κρυσταλλογραφία, νανοσωματίδια, κατασκευή Wulff, σχεδιασμός νανοσωματιδίων, ανάπτυξη διαδικτυακού εργαλείου

To my family

.

AKNOWLEDGMENTS

CONTENTS

LIST OF IMAGES

LIST OF TABLES

PREFACE

The master thesis 'A web-based crystallographic tool for the construction of nanoparticles' has been conducted at the Biomedical Research Foundation Academy of Athens for the completion of the Postgraduate Program "Information Technologies in Medicine and Biology" (I.T.M.B.), Department of Informatics and Telecommunications, National and Kapodistrian University of Athens, Greece.

The first chapter presents the motivation of the study, the application of nanoparticles (NPs) in the industry and their advantages and the several existed approaches for nanoparticle synthesis. Furthermore, the nanocrystals and the importance of their surfaces are explained. The study objectives are then defined.

In the second chapter, the theoretical foundations of the present work are presented. First, the crystallography theory is discussed, explaining the unit cell, the 7 crystal systems the 4 centering types, the 14 Bravais lattices, the 32 crystallographic point groups and the 230 crystallographic space groups. Next, the system for the Millers indices and the fractional coordinates, as well as the theory about the Wulff construction which is used in this thesis are explained.

In the third chapter, the algorithm of the tool is discussed in two another subchapters. The first is to create the equilibrium shape of the nanoparticle and the second to replicate the unit cell until the equilibrium shape is filled with atoms. In the last subchapter, the web development and the creation of the website for the tool are presented.

The results of the present thesis are presented in chapter four. First, the program use is shown, explaining all the required inputs, the implementation of the algorithm and the various outputs of the tool. Then some use cases are shown for a further understanding of the program use, along with the validation of the results showing their reliability.

Finally, the epilogue of this thesis constitutes the conclusions along with the possible future extensions of the tool.

1. INTRODUCTION

Το μέγεθος της σελίδας θα πρέπει να είναι Nanoscience primarily investigates synthesis, characterization, exploration, and exploitation of nanostructured materials. 'Nano' derives from the Greek word 'nanos', which means dwarf or extremely small and is a prefix used to describe 'one billionth', or 10^{-9}, of a unit [1]. Therefore a nanometer is a billionth of a meter or 10^{-9} m. One nanometer is approximately the length equivalent to 10 hydrogens or 5 silicon atoms aligned in a line. Nanotechnologies involve the creation and manipulation of materials at the nanometer scale, either by scaling up from single groups of atoms or by refining or reducing bulk materials.

Nanotechnology is the term given to those areas of science and engineering where phenomena that take place at dimensions in the nanometer scale are utilized in the design, characterization, production, and application of materials, structures, devices, and systems, on an atomic, molecular, and supramolecular scale. Physics Nobel laureate Richard P Feynman introduced the concept of nanotechnology in his famous lecture entitled "There's plenty of room at the bottom" at the December 1959 meeting of the American Physical Society [2], in which he described the possibility of synthesis via direct manipulation of atoms. The term "nanotechnology" was first used in 1974 by a professor at the Tokyo University of Science, Norio Taniguchi to describe extra-high precision and ultra-fine dimensions [3], though it was not widely known. Today, nanotechnology is among the fastest growing areas of science and technology, with exponential progress being made (Figure 1). By 2025, nanotechnology is expected to be a mature industry, with countless mainstream products [4].

In general, the size of a nanoparticle spans the range between 1 and 100 nm. The principal parameters of nanoparticles are their shape (including aspect ratios where appropriate), size, and the morphological sub-structure of the substance. Current knowledge of science at the nanometer scale is derived from many disciplines, originating with the atomic and molecular concepts in chemistry and physics, and then incorporating molecular life sciences, medicine, and engineering.
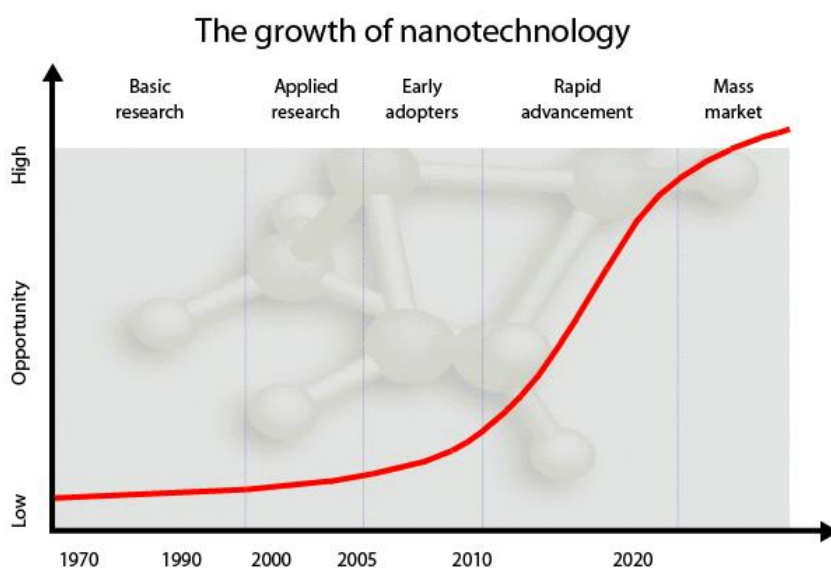
Figure 1: The growth of nanotechnology. [5]

1.1 Nanoparticle applications in industry

Nanotechnologies are now widely considered to have the potential to bring benefits in areas as diverse as drug development and drug delivery and imaging [6], water decontamination, fabrics, information and communication technologies, paints and coating, sports products and textiles, food packaging and agrochemicals etc. [7] (Figure 2). Nanoparticles can contribute to stronger, lighter, cleaner and "smarter" surfaces and systems. For example, ceramic silicon carbide nanoparticles dispersed in magnesium produce a robust and lightweight material [8] and zinc oxide nanoparticles can be dispersed in industrial coatings to protect the coating and underlying materials (i.e., substrate) from UV degradation [9]. Another example in drug delivery is the use of polymeric micelle nanoparticles to deliver drugs to tumors [10] and the synthesis and surface engineering of iron oxide nanoparticles for several biomedical applications, such as tissue repair, drug delivery and others [11]. There are many nanoparticle applications in energy and electronics too, such us coating anodes of lithium-ion batteries with silicon nanoparticles, which can increase battery power and reduce recharge time [12] and the structurally ordered intermetallic platinum-cobalt core-shell nanoparticles, which produce enhanced activity and stability as oxygen reduction electrocatalysts [13]. In 2010, more than 1000 products containing nanoparticles became commercially available [14].
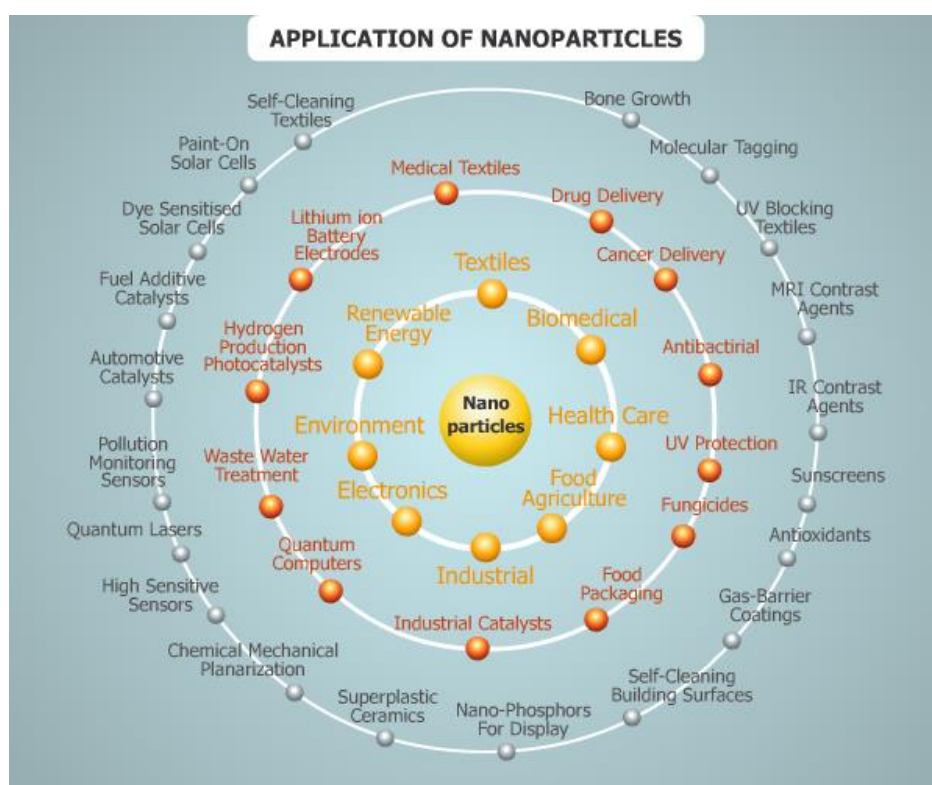
Figure 2: Applications of nanoparticle-based material. [15]

The large specific surface area of nanoparticles is the origin of a number of their unique applications [16]. Also, nanoparticles have a greater surface area per weight than larger particles, which has been found to be the reason behind many of these novel physical and chemical properties, which allow a wide range of applications with economic benefits.

1.2 Nanoparticle synthesis

Nanoparticles are formed through the natural or human-mediated disintegration of larger structures or by controlled assembly processes. There are several techniques for the preparation of nanoparticles, which can be divided into two major categories, the top-down and the bottom-up approach (Figure 3). The top-down processing has been and will be the dominant process in semiconductor manufacturing. The top-down process is when nanomaterials are synthesized by breaking down of bulk solids into nanosizes. Instead of taking material away to make structures, the bottom-up approach selectively adds atoms to create structures, so nanomaterials are synthesized by assembling atoms or molecules.
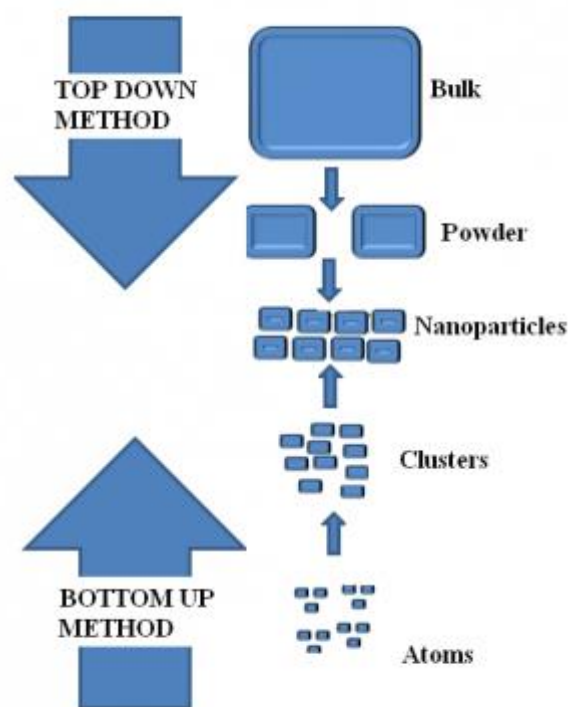
Figure 3: The two different type of approaches by which the nanoparticles are formed. [17]

The top-down approach includes the following techniques (Figure 4) [18]:

- High-energy ball milling: Milling bulk materials produce nanoscale powders. [19]

- Wire explosion: Used to produce conducting nanomaterials such as metals. A sudden high current pulse is supplied resulting in an explosion. [20]

- Arc discharge: Alternating current (AC) or direct current (DC) arcs are used to evaporate materials. [21]

- Inert-gas condensation: Particle growth is achieved by condensing evaporated atoms in a matrix. [22]

- Laser ablation: High-energy laser to induce evaporation. [23]

- Ion sputtering: Impact using high energy ions (usually rare gases) cause evaporation. [24]

On the other hand, the bottom-up approach includes the following techniques (Figure 4) [18]:

- Chemical reduction: Metal ions are reduced using reducing agents to create atoms. [25]

- Electrochemical synthesis: Electrochemical reduction or oxidation reactions. [26]

- Photochemical synthesis: Chemical processes assisted by light. [27]

- Sonochemical routes: Chemical reaction system is done with the aid of ultrasound. [28]

- Solvothermal synthesis: Chemical processes in a closed system using solvents at lower temperatures. [29]

- Interfacial synthesis: An organic-aqueous interface is created to make nanomaterials. [30]

- Micelles and microemulsions: Producing nanomaterials by using oil-in-water or water-in-oil emulsions, or cavities of micelles or reverse micelles. [31]

- Biological methods: Biomolecules or living cells being used as synthetic reactors. [32]

- Thermolysis strategies: Reactions in flames and thermal decomposition. [33]

- Arrested precipitation (mainly for semiconductors and oxides): Desired material is precipitated from an organometallic precursor solution. [34]

- Solvated metal atom dispersion (SMAD): Nanoparticles are synthesized from metal vapors deposited in solid matrices of solvents, which upon heating evaporates to create the nanostructure. Synthesis of protected clusters is also possible if a capping agent is present in the solvent used. [35]
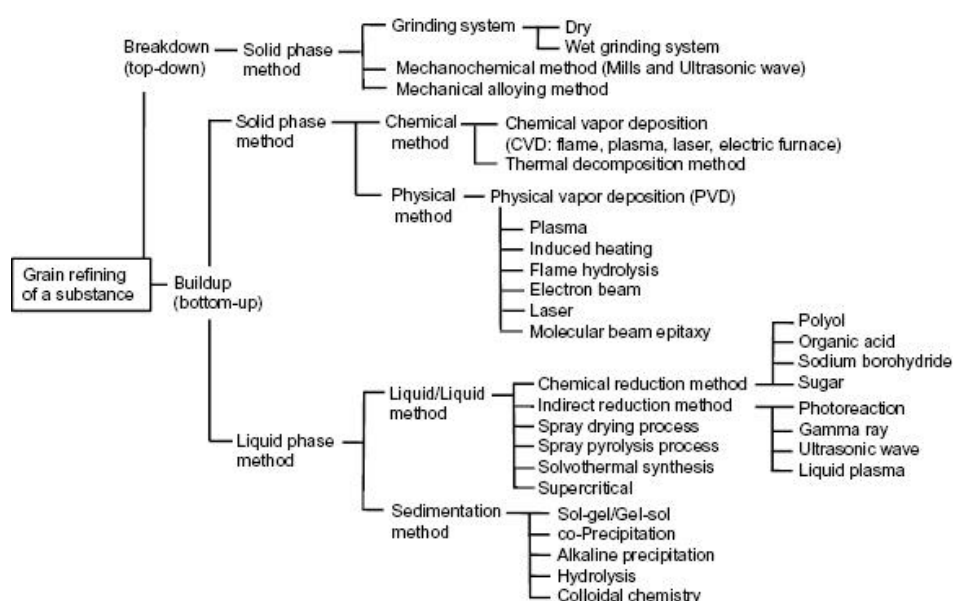
Figure 4: Typical synthetic methods for nanoparticles for the top-down and bottom-up approaches. [36]

Often a hybrid model including more than one of the above techniques is used to synthesize nanoparticles. Also, even for the same material, different methods are often used to optimize specific properties of nanoparticles such as size, size distribution, symmetry, purity, and others.

In the most recent years, computational techniques have been created to synthesize nanoparticles. Computation methodologies for modeling nanoparticles can be classified depending on the timescale and the length they apply. These methods vary from *ab-initio* quantum calculations, where very small systems for short times are modeled in the highest possible detail, to classical microscopic (atomistic) simulations, to mesoscopic coarse-graining techniques, up to macroscopic approaches where systems are modeled in the continuum description (Figure 5). In the electronic scale, quantum mechanical calculations are applied, where the density functional theory (DFT) is usually used. In the atomistic level, the techniques are most often statistical such us Monte Carlo (MC) and Molecular Dynamics (MD), which have the advantage of a detailed representation of microstructure and direct comparison with experimental data. Some examples of Molecular Dynamics simulation studies are the stability-limited growth mechanism of peptide-mediated gold nanoparticle synthesis [37], the growth mechanisms of silver nanoparticles [38] and the sintering rate and mechanism of TiO2 NPs [39]. On the other hand, a few studies using the MC technique are the equilibrium Monte Carlo simulations of A1–L10 ordering in FePt nanoparticles [40], the finite-size and surface effects in maghemite nanoparticles [41] and the growth and kinetic Monte Carlo simulation of InAs quantum wires on vicinal substrates [42]. These techniques are less demanding enabling systems of thousands of atoms to be studied for tens or hundreds nanoseconds. In these statistical methods the electronic detail is lost, but when the electron perturbation is small, this is not important [43]. In many studies like this, the Wulff construction [44] is used in order to predict the NP shape using first-principles calculations, like in this MC study, where shape and faceting of Si nanocrystals are embedded in a−SiO2 [45] and the Monte Carlo studies of equilibrium and growth shapes of a crystal [46] as well as in this MD study, where Wulff construction and molecular dynamics simulations were applied to model Au nanoparticles [47] and this systematic study of the diffusion of single adatoms and the growth of fcc silver and gold clusters (Wulff polyhedra) by MD simulations [48].
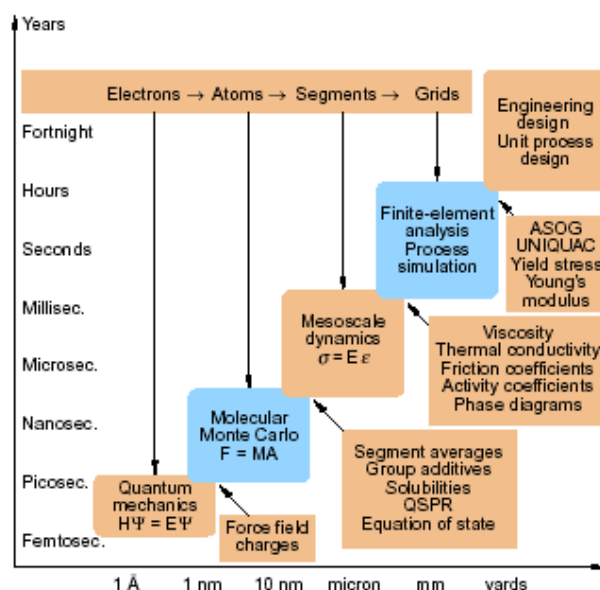
Figure 5: The timescale and length scale for the modeling of nanoparticles. [49]

1.3 Nanocrystals

Nanoparticles can be amorphous or crystalline. A crystal or crystalline solid is a solid material whose constituents (such as atoms, molecules, or ions) are arranged in a highly ordered microscopic structure, forming a crystal lattice that extends in all directions. A crystalline nanoparticle or nanocrystal is a crystal having at least one dimension smaller than 100 nanometers. All nanomaterials share a common feature of large surface-to-volume ratio, making their surfaces the dominant player in many physical and chemical processes. Surface ligands, molecules that bind to the surface, are an essential component of nanomaterial synthesis, processing, and application. Understanding the structure and properties of nanoscale interfaces requires an intricate mix of concepts and techniques borrowed from surface science and coordination chemistry [50].The dimensions of nanocrystals are so close to atomic dimensions that an unusually high fraction of the total atoms would be present on their surfaces. A nanocrystal has a surface more populated than the bulk [51] (Figure 6). It is possible to estimate the fraction of atoms on the surface of pseudo-spherical nanocrystals (P_s, percentage) using the simple relation,

$$P_s = 4N^{-1/3} \times 100 \qquad (1)$$

where N is the total number of atoms in the particle [52].
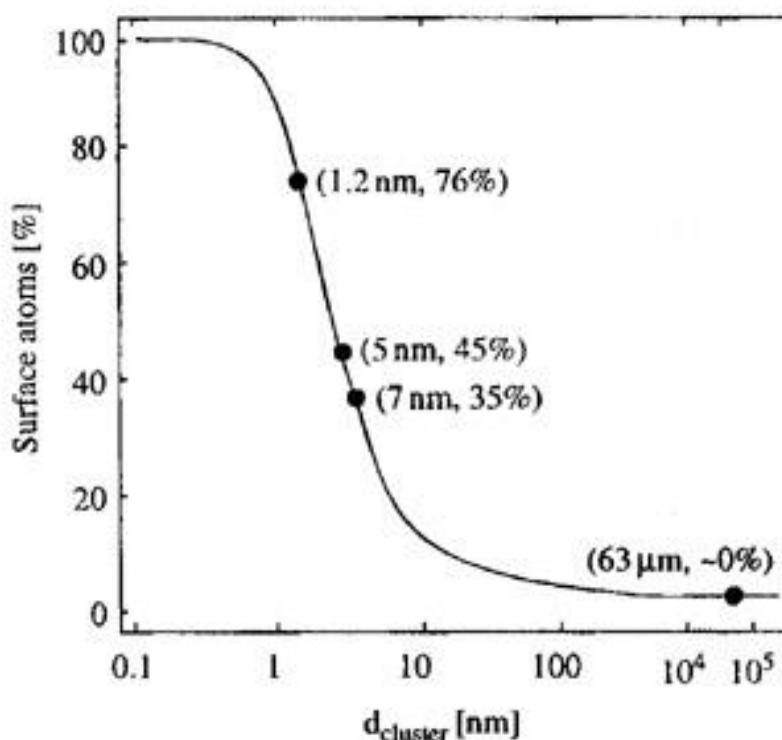
Figure 6: Percentage of surface atoms as a function of cluster diameter of Palladium clusters. [53]

1.4 Study Objectives

Crystals of materials form nanoparticles, so individual crystals grow based on their crystal habits, which give the characteristic external shape of a crystal, but crystallographic files contain only the crystal structure and not its crystal shape. However, creating an initial starting conformation for modeling and simulation is tedious, because every crystalline material grows with a different crystal habit and different symmetry in nature. That gave us the motivation to provide the first easily accessible web-based crystallographic tool, without installation or sign up, which can produce nanoparticles for simulation from any material as they grow in nature of any type, any size, and any shape.

The study objectives can be split up into two aims (Figure 7):

Aim 1. Determine the equilibrium shape of the nanoparticle according to its crystal habit, crystal parameters, crystal point group and maximum making use of the Quickhull algorithm.

Aim 2. Fill the equilibrium shape with atoms by translating the unit cell across all three spatial directions. As a result, the nanoparticle is constructed, and the coordinates of the atoms are output to the user.
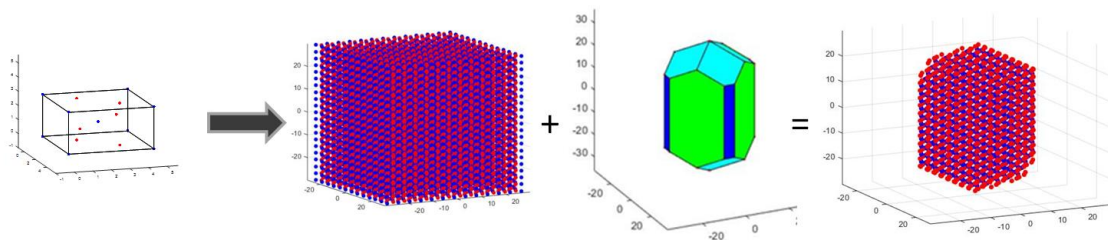
Figure 7: A graphical overview of the study objectives.

2. CRYSTALLOGRAPHY THEORY

Crystallography is the experimental science concerned with the structure and properties of the crystalline state, determining the arrangement of atoms in the crystalline solids. A crystallographer is a scientist in this discipline who uses X-ray or neutron diffraction to build pictorial representations (or models) of a crystalline solid. Each crystal in a crystalline solid is composed of a single arrangement of atoms that repeats, like building blocks, throughout three-dimensional space, where the smallest repeating pattern is called the unit cell. The space group of the crystal, in turn, describes the symmetry of the repeating pattern in the crystal. A space group is a way of describing the arrangement of the repeating patterns in a crystal using a standardized system of notation. X-ray structure determination is beneficial because the three-dimensional structure of a molecule can be represented at atomic resolution. Therefore it is almost always a principal goal of an experimental chemist to obtain a crystal structure (i.e., a structural representation) of every compound, especially in modern drug design. The science of determining crystal structure models (crystallography) has grown significantly over the past 100 years. Since the solving of the first crystal structure (CuSO4), crystallography has been used to study the structural features of the simple inorganic compounds to enhance the understanding of fundamental inorganic principles. This introduction will focus on the science of crystallography.

2.1   Unit cell

The unit cell is the smallest group of particles in a material. It is a box formed of one or more atoms and molecules arranged in three dimensions that constitute the repeating pattern of the crystal structure. So, the whole crystal structure is formed by repetitive translation of the unit cell across all three spatial directions. The unit cell also defines the symmetry and the structure of the entire crystal lattice. The opposite faces of a unit cell are always parallel, and the edges connect equivalent points.
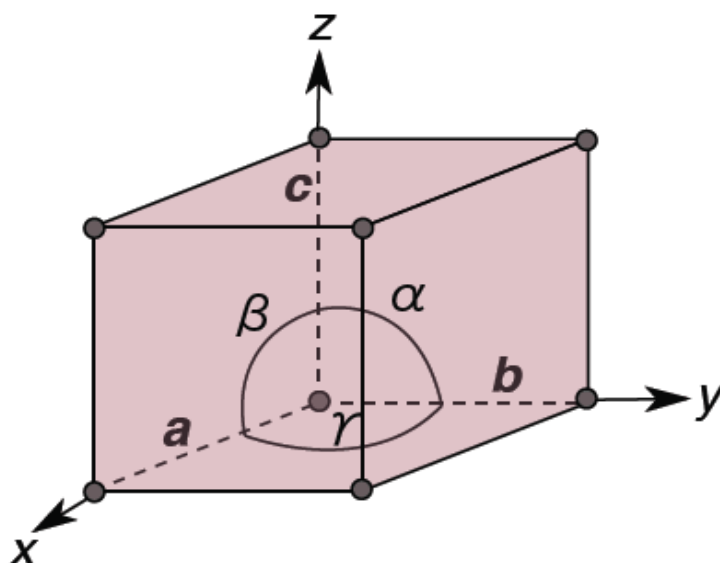
Figure 8: The unit cell with lengths a, b, and c and angles α, β, and γ. [54]

The length of the principal axes a, b and c of the unit cell and the angles α, β and γ (alpha, beta and gamma) between them are the lattice constants, also called lattice parameters (Figure 8).

2.2 Crystal structure

The crystal structure is defined as a combination of the crystal lattice with the motif (or else base), so we need to define the latter two. A lattice, in general, is defined as a discrete but infinite regular arrangement of points in a vector space [55]. The lattice can then be described as a linear combination, of the independent vectors α_1, α_2 and α_3 with m, n and o being their respective integer coefficients in the R^3, as it is shown in the following equation:

$$\vec{T}_{mno} = m\vec{\alpha}_1 + n\vec{\alpha}_2 + o\vec{\alpha}_3 \quad m, n, o \in \mathbb{Z} \quad (2)$$

A crystal lattice is a lattice where its points are the connection points between the unit cells (Figure 9). These points are called lattice points.
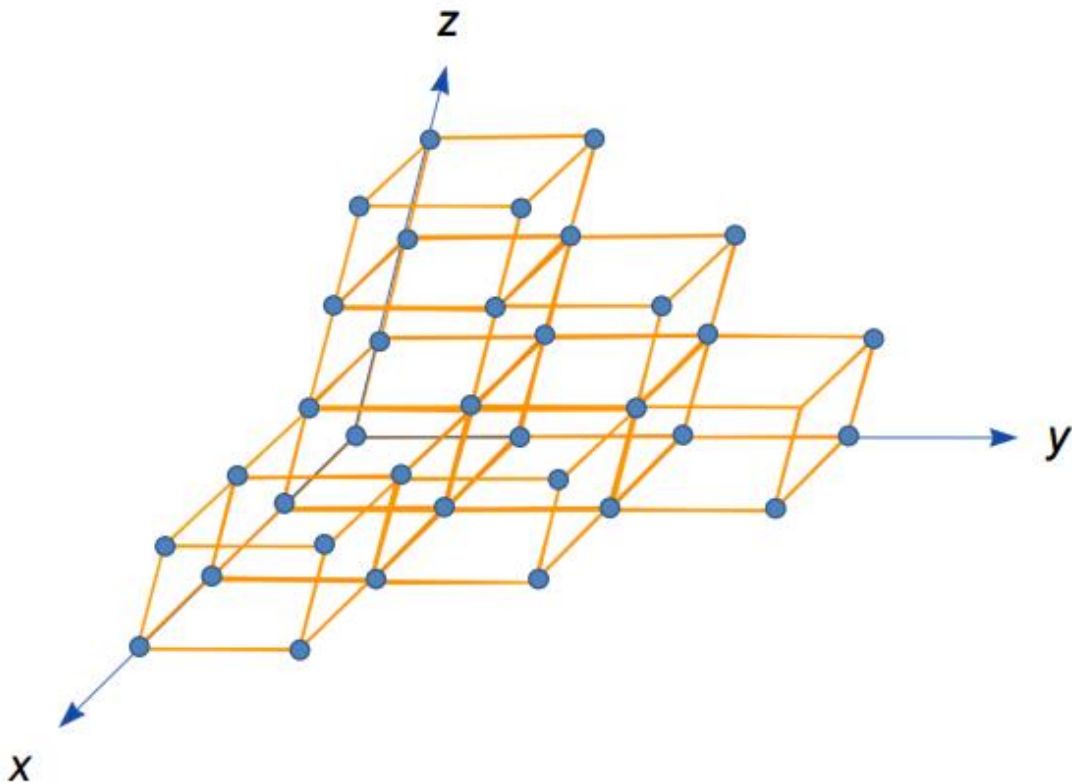
Figure 9: The connection points between the unit cells form the crystal lattice. [56]

The motif, or else basis, consists of the arrangement of the building blocks (atoms, molecules) of a unit cell. If we replace the lattice points with the motif, we obtain the crystal structure (Figure 10), with all building blocks being subject to the same translation principle [57].
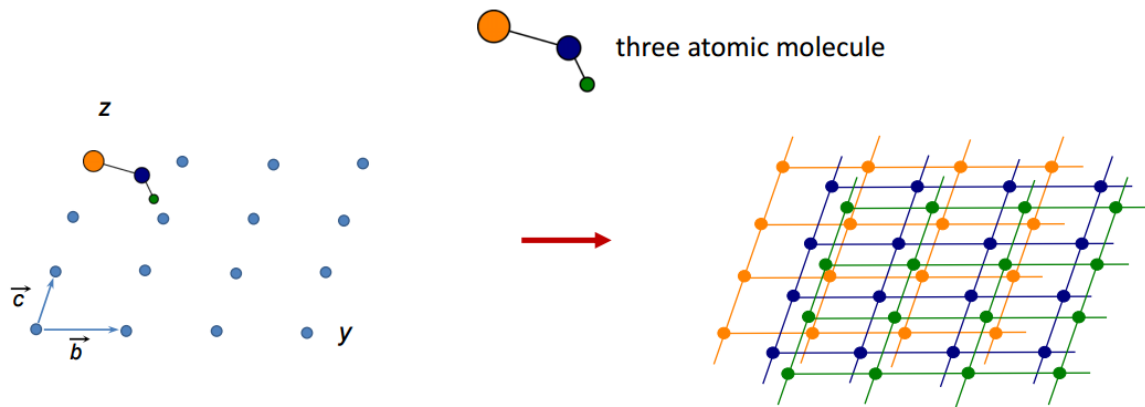
Figure 10: Crystal lattice + Motif = Crystal structure. [56]

To sum up, the unique arrangement of atoms or molecules in a crystalline material is called crystal structure [58].

2.3 Crystal systems

The structures of all crystals can be classified according to the symmetry of the unit cells. There are 7 of these groups, where every possible crystal structure of the world belongs and are called crystal systems. The symmetry of each crystal system is described by the relationship between the lattice lengths a, b, and c and angles α, β, and γ.

restrictions *for*	cell constants	cell angles
triclinic	none	none
monoclinic	none	$\alpha = \gamma = 90°$
orthorhombic	none	$\alpha = \beta = \gamma = 90°$
tetragonal	a = b	$\alpha = \beta = \gamma = 90°$
trigonal	a = b	$\alpha = \beta = 90°; \gamma = 120°$
hexagonal	a = b	$\alpha = \beta = 90°; \gamma = 120°$
cubic	a = b = c	$\alpha = \beta = \gamma = 90°$

symmetry

hexagonal crystal *family*

Figure 11: The 7 possible crystal systems. [59]

In Figure 11 we see the 7 possible crystal systems in ascending symmetry, each one having its restrictions for its unit cell parameters, which are:

- The triclinic with no restrictions,

- The monoclinic with restriction of unit cell angles α and γ being equal to 90°.

- The orthorhombic with restriction of unit cell angles α, β, and γ being equal to 90°.

- The tetragonal with restriction of unit cell lengths a and b being equal and unit cell angles α, β, and γ being equal to 90°.

- The trigonal and the hexagonal with restriction of unit cell lengths a and b being equal, unit cell angles α and β being equal to 90° and unit cell angle being equal to 120°.

- The cubic with restriction of unit cell lengths a, b, and c being equal and unit cell angles α, β, and γ being equal to 90°.

2.4 Centering types

Every crystal structure is also represented by a centering type which shows the position (which can be described by equation (2)) of the atoms or molecules (lattice points) in the unit cell. There are 4 different centering types, the primitive, the base-centered, the body-centered and the face-centered, which belong to all crystal systems and an additional one, the rhombohedral-centered which only applies for the hexagonal crystal family.

The primitive (P) has an atom or a molecule on the cell corners only. The rest of the centering types are like the primitive with the difference that the base-centered (A, B, or C) has one additional atom or molecule at the center of each face of one pair of parallel faces of the cell, the body-centered (I) has one additional atom or molecule at the center of the cell, the face-centered (F) has one additional atom or molecule at the center of each of the faces of the cell and the rhombohedrally-centered (R) which again only applies to the hexagonal crystal family has two additional atoms or molecules along the longest body diagonal [60]. All of the above are shown in Figure 12.
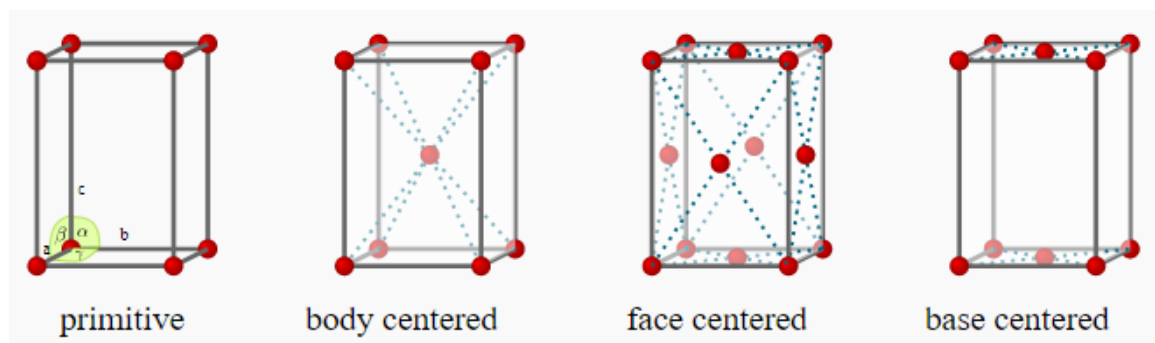
Figure 12: The 4 centering types showing the position of the lattice points. [61]

2.5 Bravais lattices

The combination of the 7 crystal systems with the centering types has, as a result, the Bravais lattices that are the distinct lattice types which when repeated can fill the whole space [62]. The Bravais lattices are 14 in total, and that is because some of the other 14 are either redundant or are not possible due to symmetry reasons. For example, there are 4 tetragonal Bravais lattices which are a combination of the tetragonal crystal system with all 4 centering types, but on the other hand, there is only one triclinic

Bravais lattice which is a combination of the triclinic crystal system with the primitive centering type. The 14 Bravais lattices are shown in Figure 13.
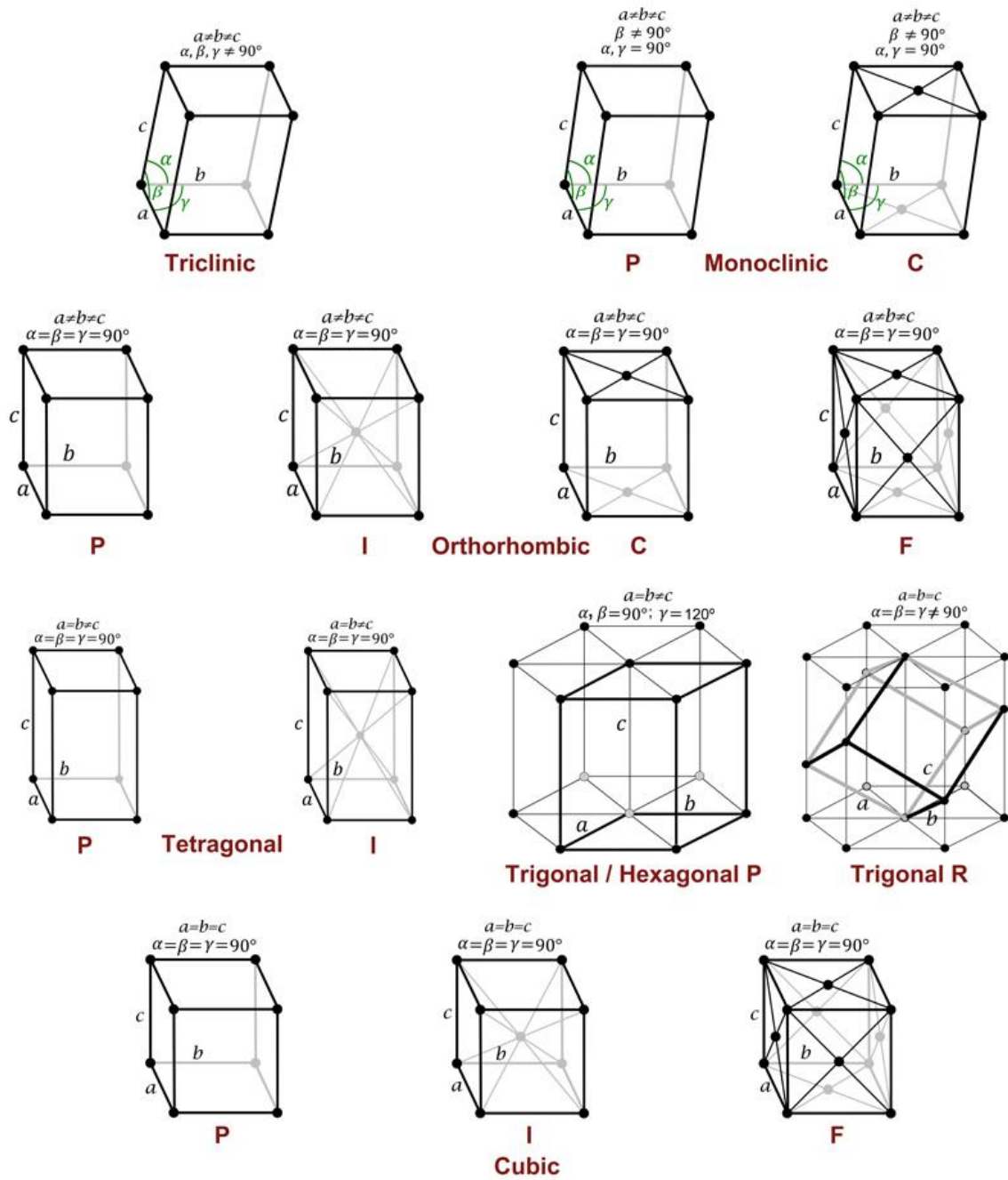
Figure 13: The 14 Bravais lattices. [63]

2.6   Point groups

To define point groups, we need to describe the symmetry operation theory. When a symmetry operation is applied on an atom with coordinates (x_1, y_1, z_1), the same atom with identical surroundings is created with atomic coordinates (x_2, y_2, z_2). There are 4 essential symmetry elements (Figure 14) which are:

- The Identity, which leaves the atom to the same position and is included because it is a requirement in point group theory.

- The Rotation axis, which rotates an object $360^{o}/n$ with the n-fold axis being equal to 1, 2, 3, 4 and 6 because any other value of n is invalid in crystallographic point group theory.

- The Inversion, which translates the atomic coordinates to the opposite direction that is from (x, y, z) to (-x, -y, -z). When an object has that symmetry element, it is called centrosymmetric.

- The Mirror plane (reflection), which naturally acts as a mirror and places the object on the other side of a mirror axis. For example, if the yz plane is a mirror plane, the atom is transferred from (x, y, z) to (-x, y, z).

A crystallographic point group is a group of symmetry operations, like rotations or reflections, all of which leave at least one central point fixed while moving other directions and faces of the crystal to the positions of features of the same kind. The simplest crystallographic point groups are the single n-fold rotation axis with n = 1, 2, 3, 4, and 6. Likewise, the rotary-inversion axes (a combination of the rotation axis and inversion symmetry elements) are the basis for the point groups -1, -2 (or else called m), -3, -4, and -6. The remaining 22 crystallographic point groups result from the combination of the previous 10 point groups. Often the minus symbol is replaced with a bar above the n-fold number. A slash character before the symbol m indicates a mirror plane perpendicular to the main axis of rotation. The 32 crystallographic point groups which are divided into the 7 crystal systems can be viewed in Figure 15, and the relationship between each other is shown in Figure 16 with group order from bottom to top of 1, 2, 3, 4, 6, 8, 12, 16, 24 and 48 respectively [65, 66].
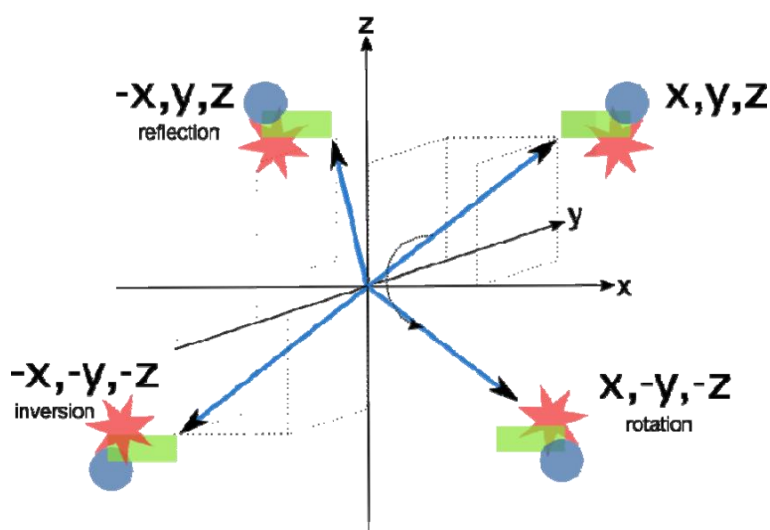
Figure 14: The operations of symmetry: rotation, inversion, and reflection (mirror plane). [67]

Class	Group names						
Cubic	23	m$\bar{3}$		432	$\bar{4}$3m	m$\bar{3}$m	
Hexagonal	6	$\bar{6}$	$^6\!/_m$	622	6mm	$\bar{6}$2m	$^6\!/_m$mm
Trigonal	3	$\bar{3}$		32	3m	$\bar{3}$m	
Tetragonal	4	$\bar{4}$	$^4\!/_m$	422	4mm	$\bar{4}$2m	$^4\!/_m$mm
Monoclinic Orthorhombic	2		$^2\!/_m$	222	m	mm2	mmm
Triclinic	1	$\bar{1}$					

Figure 15: The 32 crystallographic point groups. [68]
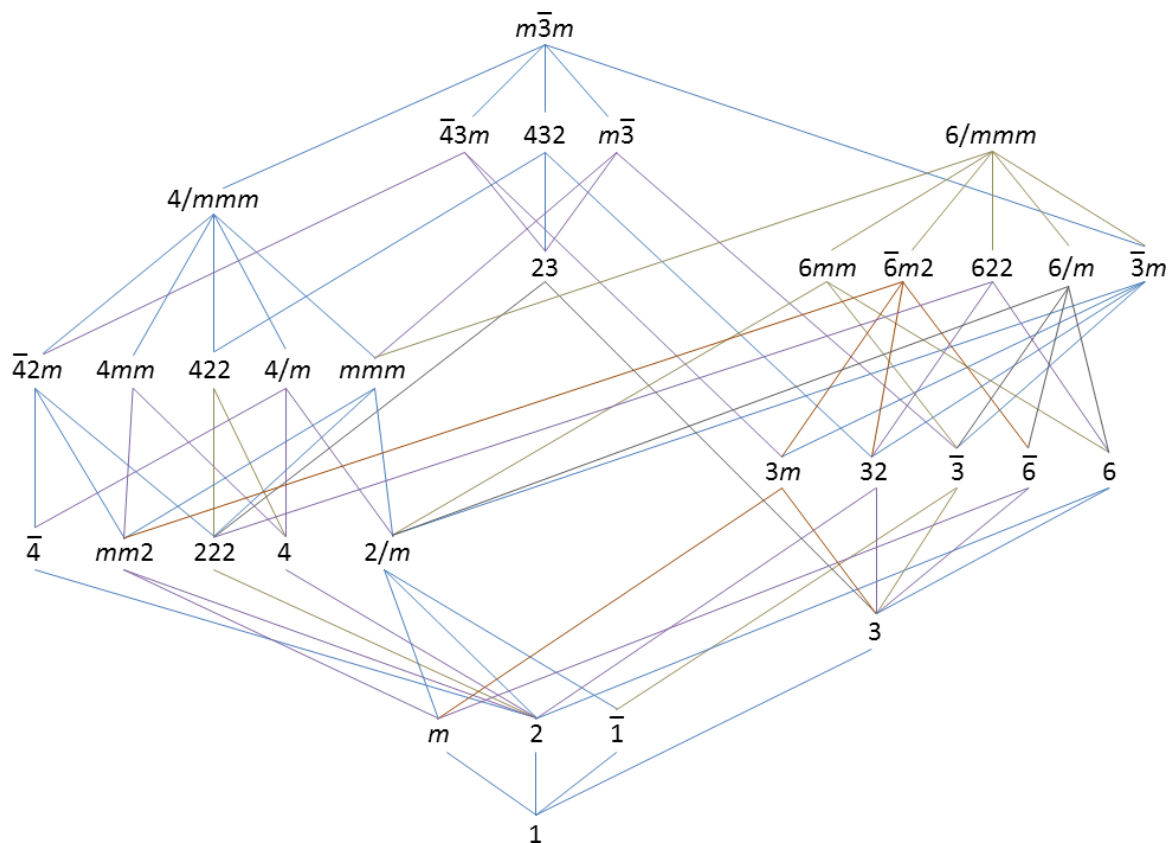
Figure 16: The relationship between the point groups. [68]

2.7 Space groups

The combination of the 14 Bravais lattices with the 32 point groups gives rise to the space groups, which ultimately defines the symmetry of a crystal. Space groups are 230 in total in the 3-dimensional space and are a combination of the translational symmetry of a unit cell including lattice centering and the point group symmetry operations. In addition to the symmetry operations that were already described, here we introduce another two symmetry elements which are not applicable to the point groups but are in space groups [69] (Figure 17). These are:

- The Glide planes, which is a reflection in a plane, followed by a translation parallel with that plane. These are noted by a, b, or c, depending on which axis the glide is along. These are called axial glide planes and involve mirroring combined with a translation 1/2 along an axis. There is also the n glide which is along the half of a diagonal of a face and is called diagonal glide plane, and there is also the d glide which is a glide along either a face or space diagonal of the unit cell and is called diamond glide planes.

- The Screw axis, which is a rotation about an axis, followed by a translation along the direction of the axis. These have the notation n_m where n is the rotation axis "fold," and m/n is the translation given as a fraction of the unit translation parallel to the rotation axis. For example, 2_1 is a twofold rotation followed by a translation of 1/2 of the lattice vector.
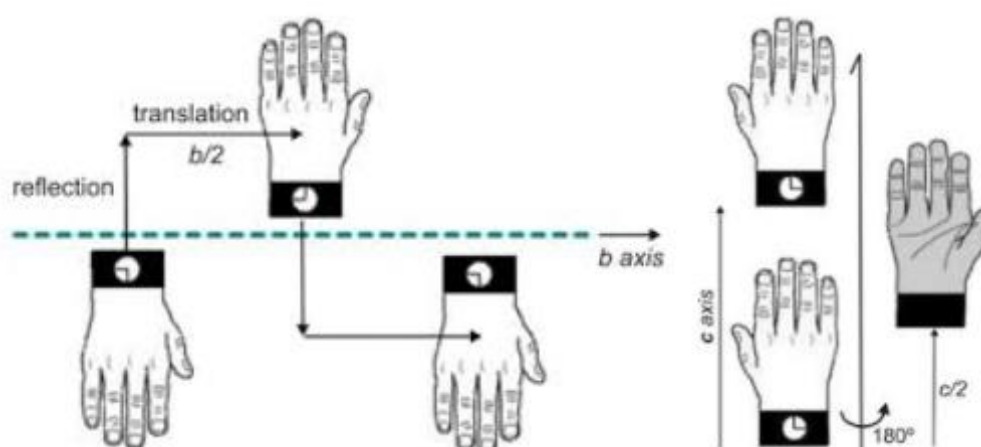
Figure 17: A glide plane on the left and a twofold screw axis on the right. [70]

In mathematics, the application of symmetry operations is a sequence of matrix multiplications. For example, in Figure 19 first the inversion symmetry element is applied to a vector which might represent an atom or a plane. Then a 2-fold rotation about the b-axis is applied, where again an n-fold rotation is a rotation of $360°/n$, so a 2-fold rotation is a rotation of $180°$. In the end we have a translation of 1 in the a axis, a translation of 2 in the b axis, and a translation of 3 in the c axis. As a result we obtain a new vector symmetric to the starting one, according to the above symmetry operation.

$$\begin{pmatrix} x' \\ y' \\ z' \\ 1 \end{pmatrix} = \begin{pmatrix} 1 & 0 & 0 & 1 \\ 0 & 1 & 0 & 2 \\ 0 & 0 & 1 & 3 \\ 0 & 0 & 0 & 1 \end{pmatrix} \begin{pmatrix} \cos\pi & 0 & -\sin\pi & 0 \\ 0 & 1 & 0 & 0 \\ \sin\pi & 0 & \cos\pi & 0 \\ 0 & 0 & 0 & 1 \end{pmatrix} \begin{pmatrix} -1 & 0 & 0 & 0 \\ 0 & -1 & 0 & 0 \\ 0 & 0 & -1 & 0 \\ 0 & 0 & 0 & 1 \end{pmatrix} \begin{pmatrix} x \\ y \\ z \\ 1 \end{pmatrix}$$

$$\underbrace{\qquad}_{\text{Translation}} \qquad \underbrace{\qquad}_{\text{Rotation}} \qquad \underbrace{\qquad}_{\text{Inversion}}$$

Figure 18: Application of inversion followed by a 2-fold rotation about the b-axis and followed by a translation of [123]. [71]

From the 230 space groups, the 73 are the output from combinations of the 14 Bravais lattices and the 32 crystallographic point groups without any extra symmetry operations such as screw axes and glide planes being involved. These space groups are called symmorphic and the other 157 nonsymmorphic space groups. In Figure 19 there is a summary of how the space groups are produced.
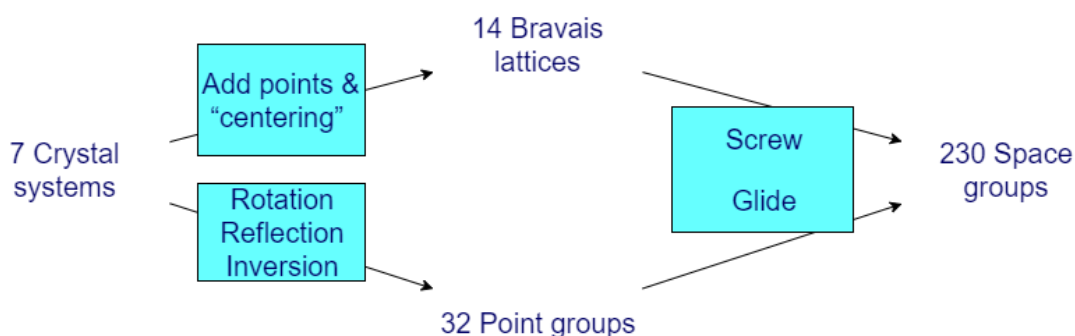
Figure 19: A summary of the space groups' production.

A space group is described by a capital letter to identify the Bravais lattice type (such as P, C, and F) followed by the point group symbols in which rotation and reflection symmetry is followed by the screw axes and glide planes. The effects that symmetry has on a unit cell is usually referenced to an arbitrary point x, y, z. The elements of symmetry for a specific point group act on the point and produce a list of equivalent positions. In Figures 20 and 21 the 230 space groups can be viewed.

Table 1-1
Symbols for the 230 space groups.   Notation is described in the text

Triclinic

1. C_1^1 (P1)
2. C_i^1 (P$\bar{1}$)

Monoclinic

3. C_2^1 (P2)
4. C_2^2 (P2$_1$)
5. C_2^3 (B2)
6. C_s^1 (Pm)
7. C_s^2 (Pb)
8. C_s^3 (Bm)
9. C_s^4 (Bb)
10. C_{2h}^1 (P2/m)
11. C_{2h}^2 (P2$_1$/m)
12. C_{2h}^3 (B2/m)
13. C_{2h}^4 (P2/b)
14. C_{2h}^5 (P2$_1$/b)
15. C_{2h}^6 (B2/b)

Orthorhombic

16. D_2^1 (P222)
17. D_2^2 (P222$_1$)
18. D_2^3 (P2$_1$2$_1$2)
19. D_2^4 (P2$_1$2$_1$2$_1$)
20. D_2^5 (C222$_1$)
21. D_2^6 (C222)
22. D_2^7 (F222)
23. D_2^8 (I222)
24. D_2^9 (I2$_1$2$_1$2$_1$)
25. C_{2v}^1 (Pmm2)
26. C_{2v}^2 (Pmc2$_1$)
27. C_{2v}^3 (Pcc2)
28. C_{2v}^4 (Pma2)
29. C_{2v}^5 (Pca2$_1$)
30. C_{2v}^6 (Pnc2)
31. C_{2v}^7 (Pmn2$_1$)
32. C_{2v}^8 (Pba2)
33. C_{2v}^9 (Pna2$_1$)
34. C_{2v}^{10} (Pnn2)
35. C_{2v}^{11} (Cmm2)

36. C_{2v}^{12} (Cmc2$_1$)
37. C_{2v}^{13} (Ccc2)
38. C_{2v}^{14} (Amm2)
39. C_{2v}^{15} (Abm2)
40. C_{2v}^{16} (Ama2)
41. C_{2v}^{17} (Aba2)
42. C_{2v}^{18} (Fmm2)
43. C_{2v}^{19} (Fdd2)
44. C_{2v}^{20} (Imm2)
45. C_{2v}^{21} (Iba2)
46. C_{2v}^{22} (Ima2)
47. D_{2h}^1 (Pmmm)
48. D_{2h}^2 (Pnnn)
49. D_{2h}^3 (Pccm)
50. D_{2h}^4 (Pban)
51. D_{2h}^5 (Pmma)
52. D_{2h}^6 (Pnna)
53. D_{2h}^7 (Pmna)
54. D_{2h}^8 (Pcca)
55. D_{2h}^9 (Pbam)
56. D_{2h}^{10} (Pccn)
57. D_{2h}^{11} (Pbcm)
58. D_{2h}^{12} (Pnnm)
59. D_{2h}^{13} (Pmmn)
60. D_{2h}^{14} (Pbcn)
61. D_{2h}^{15} (Pbca)
62. D_{2h}^{16} (Pnma)
63. D_{2h}^{17} (Cmcm)
64. D_{2h}^{18} (Cmca)
65. D_{2h}^{19} (Cmmm)
66. D_{2h}^{20} (Cccm)
67. D_{2h}^{21} (Cmma)
68. D_{2h}^{22} (Ccca)
69. D_{2h}^{23} (Fmmm)
70. D_{2h}^{24} (Fddd)
71. D_{2h}^{25} (Immm)
72. D_{2h}^{26} (Ibam)
73. D_{2h}^{27} (Ibca)
74. D_{2h}^{28} (Imma)

Tetragonal

75. C_4^1 (P4)
76. C_4^2 (P4$_1$)
77. C_4^3 (P4$_2$)
78. C_4^4 (P4$_3$)
79. C_4^5 (I4)
80. C_4^6 (I4$_1$)
81. S_4^1 (P$\bar{4}$)
82. S_4^2 (I$\bar{4}$)
83. C_{4h}^1 (P4/m)
84. C_{4h}^2 (P4$_2$/m)
85. C_{4h}^3 (P4/n)
86. C_{4h}^4 (P4$_2$/n)
87. C_{4h}^5 (I4/m)
88. C_{4h}^6 (I4$_1$/a)
89. D_4^1 (P422)
90. D_4^2 (P42$_1$2)
91. D_4^3 (P4$_1$22)
92. D_4^4 (P4$_1$2$_1$2)
93. D_4^5 (P4$_2$22)
94. D_4^6 (P4$_2$2$_1$2)
95. D_4^7 (P4$_3$22)
96. D_4^8 (P4$_3$2$_1$2)
97. D_4^9 (I422)
98. D_4^{10} (I4$_1$22)
99. C_{4v}^1 (P4mm)
100. C_{4v}^2 (P4bm)
101. C_{4v}^3 (P4$_2$cm)
102. C_{4v}^4 (P4$_2$nm)
103. C_{4v}^5 (P4cc)
104. C_{4v}^6 (P4nc)
105. C_{4v}^7 (P4$_2$mc)
106. C_{4v}^8 (P4$_2$bc)
107. C_{4v}^9 (I4mm)
108. C_{4v}^{10} (I4cm)
109. C_{4v}^{11} (I4$_1$md)
110. C_{4v}^{12} (I4$_1$cd)
111. D_{2d}^1 (P$\bar{4}$2m)
112. D_{2d}^2 (P$\bar{4}$2c)
113. D_{2d}^3 (P$\bar{4}$2$_1$m)

Figure 20: The first 113 space groups. [72]

Table 1-1 (Continued)

114. D_{2d}^4 ($P\bar{4}2_1c$)
115. D_{2d}^5 ($P\bar{4}m2$)
116. D_{2d}^6 ($P\bar{4}c2$)
117. D_{2d}^7 ($P\bar{4}b2$)
118. D_{2d}^8 ($P\bar{4}n2$)
119. D_{2d}^9 ($I\bar{4}m2$)
120. D_{2d}^{10} ($I\bar{4}c2$)
121. D_{2d}^{11} ($I\bar{4}2m$)
122. D_{2d}^{12} ($I\bar{4}2d$)
123. D_{4h}^1 ($P4/mmm$)
124. D_{4h}^2 ($P4/mcc$)
125. D_{4h}^3 ($P4/nbm$)
126. D_{4h}^4 ($P4/nnc$)
127. D_{4h}^5 ($P4/mbm$)
128. D_{4h}^6 ($P4/mnc$)
129. D_{4h}^7 ($P4/nmm$)
130. D_{4h}^8 ($P4/ncc$)
131. D_{4h}^9 ($P4_2/mmc$)
132. D_{4h}^{10} ($P4_2/mcm$)
133. D_{4h}^{11} ($P4_2/nbc$)
134. D_{4h}^{12} ($P4_2/nnm$)
135. D_{4h}^{13} ($P4_2/mbc$)
136. D_{4h}^{14} ($P4_2/mnm$)
137. D_{4h}^{15} ($P4_2/nmc$)
138. D_{4h}^{16} ($P4_2/ncm$)
139. D_{4h}^{17} ($I4/mmm$)
140. D_{4h}^{18} ($I4/mcm$)
141. D_{4h}^{19} ($I4_1/amd$)
142. D_{4h}^{20} ($I4_1/acd$)

Trigonal

143. C_3^1 ($P3$)
144. C_3^2 ($P3_1$)
145. C_3^3 ($P3_2$)
146. C_3^4 ($R3$)
147. C_{3i}^1 ($P\bar{3}$)
148. C_{3i}^2 ($R\bar{3}$)
149. D_3^1 ($P312$)
150. D_3^2 ($P321$)
151. D_3^3 ($P3_112$)
152. D_3^4 ($P3_121$)
153. D_3^5 ($P3_212$)
154. D_3^6 ($P3_221$)
155. D_3^7 ($R32$)
156. C_{3v}^1 ($P3m1$)
157. C_{3v}^2 ($P31m$)
158. C_{3v}^3 ($P3c1$)
159. C_{3v}^4 ($P31c$)
160. C_{3v}^5 ($R3m$)
161. C_{3v}^6 ($R3c$)
162. D_{3d}^1 ($P\bar{3}1m$)
163. D_{3d}^2 ($P\bar{3}1c$)
164. D_{3d}^3 ($P\bar{3}m1$)
165. D_{3d}^4 ($P\bar{3}c1$)
166. D_{3d}^5 ($R\bar{3}m$)
167. D_{3d}^6 ($R\bar{3}c$)

Hexagonal

168. C_6^1 ($P6$)
169. C_6^2 ($P6_1$)
170. C_6^3 ($P6_5$)
171. C_6^4 ($P6_2$)
172. C_6^5 ($P6_4$)
173. C_6^6 ($P6_3$)
174. C_{3h}^1 ($P\bar{6}$)
175. C_{6h}^1 ($P6/m$)
176. C_{6h}^2 ($P6_3/m$)
177. D_6^1 ($P622$)
178. D_6^2 ($P6_122$)
179. D_6^3 ($P6_522$)
180. D_6^4 ($P6_222$)
181. D_6^5 ($P6_422$)
182. D_6^6 ($P6_322$)
183. C_{6v}^1 ($P6mm$)
184. C_{6v}^2 ($P6cc$)
185. C_{6v}^3 ($P6_3cm$)
186. C_{6v}^4 ($P6_3mc$)
187. D_{3h}^1 ($P\bar{6}m2$)
188. D_{3h}^2 ($P\bar{6}c2$)
189. D_{3h}^3 ($P\bar{6}2m$)
190. D_{3h}^4 ($P\bar{6}2c$)
191. D_{6h}^1 ($P6/mmm$)
192. D_{6h}^2 ($P6/mcc$)
193. D_{6h}^3 ($P6_3/mcm$)
194. D_{6h}^4 ($P6_3/mmc$)

Cubic

195. T^1 ($P23$)
196. T^2 ($F23$)
197. T^3 ($I23$)
198. T^4 ($P2_13$)
199. T^5 ($I2_13$)
200. T_h^1 ($Pm3$)
201. T_h^2 ($Pn3$)
202. T_h^3 ($Fm3$)
203. T_h^4 ($Fd3$)
204. T_h^5 ($Im3$)
205. T_h^6 ($Pa3$)
206. T_h^7 ($Ia3$)
207. O^1 ($P432$)
208. O^2 ($P4_232$)
209. O^3 ($F432$)
210. O^4 ($F4_132$)
211. O^5 ($I432$)
212. O^6 ($P4_332$)
213. O^7 ($P4_132$)
214. O^8 ($I4_132$)
215. T_d^1 ($P\bar{4}3m$)
216. T_d^2 ($F\bar{4}3m$)
217. T_d^3 ($I\bar{4}3m$)
218. T_d^4 ($P\bar{4}3n$)
219. T_d^5 ($F\bar{4}3c$)
220. T_d^6 ($I\bar{4}3d$)
221. O_h^1 ($Pm3m$)
222. O_h^2 ($Pn3n$)
223. O_h^3 ($Pm3n$)
224. O_h^4 ($Pn3m$)
225. O_h^5 ($Fm3m$)
226. O_h^6 ($Fm3c$)
227. O_h^7 ($Fd3m$)
228. O_h^8 ($Fd3c$)
229. O_h^9 ($Im3m$)
230. O_h^{10} ($Ia3d$)

Figure 21: The rest 117 space groups. [72]

2.8 Miller indices

Miller indices form a notation system in crystallography for planes in crystal (Bravais) lattices. The orientation of a surface or a crystal plane may be defined by considering how the plane (or indeed any parallel plane) intersects the main crystallographic axes of the solid. The application of a set of rules leads to the assignment of the Miller Indices which are determined by three integers h, k, and ℓ (hkl) which quantify the intercepts and thus may be used to uniquely identify a family of lattice planes or surfaces orthogonal to $hb_1 + kb_2 + lb_3$, where b_i is the basis of the reciprocal lattice vectors. The integers are usually written in lowest terms, i.e., their greatest common divisor should be 1, and the negative integers usually can be seen written with a bar above the number. The notation {hkℓ} denotes indices of a set of all symmetrically equivalent crystal faces ('crystal form'), or net planes (Figure 22). The notation [hkℓ] or [uvw] denotes a direction on the basis of the direct lattice vectors instead of the reciprocal lattice. The notation <hkℓ> or <uvw> denotes indices of a set of all symmetrically equivalent lattice directions [hkℓ] [73].

The usage of Miller indices can be a little bit confusing to understand, but its usage is beneficial because using reciprocals spares us the complication of infinite intercepts. Formulas involving Miller indices are very similar to related formulas from analytical geometry. Specifying dimensions in unit cell terms means that the same label can be applied to any face with a similar stacking pattern, regardless of the crystal class of the crystal.

Figure 22: A crystal shape produced by {111} and {113}. [74]

Some general principles are that Miller indices are almost always small. If a Miller index is zero, then the plane is parallel to that axis. The smaller a Miller index, the more nearly parallel the plane to the axis and on the other hand the higher a Miller index, the more nearly perpendicular a plane is to that axis. Multiplying or dividing a Miller index by a constant does not affect the orientation of the plane.

A plane that cuts through the x-, y- and z-axes (parallel to the a-, b-, and c-axes for the unit cell) can generally be described through x/u + y/v + z/w = 1 where u, v, and w

represent the values of where the plane intersects the three axes. Then the Miller indices are given by h = 1/u, k = 1/v and l = 1/w. To find the Miller indices the steps are:

Step 1: Determine the intercepts of the face along the crystallographic axes, regarding the unit cell dimensions. For example, let us consider a plane on a cubic system which is parallel to the y- and z-axes and has one intercept on the x-axis at x = a (at the point (a,0,0). So the intercepts are a, ∞ and ∞.

Step 2: Take the reciprocals. In our case 1/a, 0 and 0.

Step 3: Clear fractions. By multiplying with unit cell length a, we obtain 1, 0 and 0.

Step 4: Reduce to lowest terms. We already have the lowest terms, so the Miller indices are (100) (Figure 23).
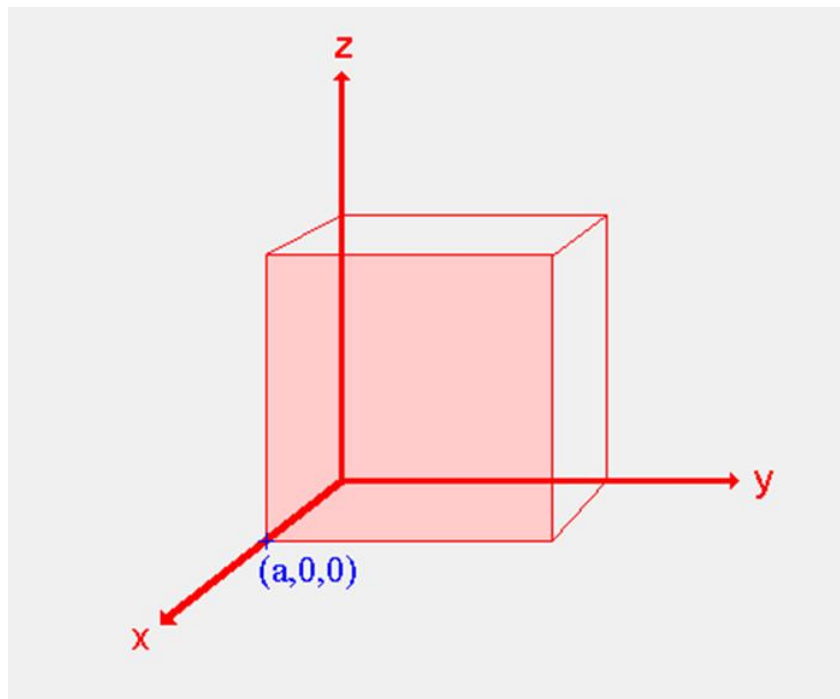
Figure 23: The (100) Miller plane in a cubic structure. [75]

On the other hand, in order to find the intercepts given miller indices, for example (210) plane on a cubic unit cell (unit cell lengths = a), the following procedure must be followed:

Step 1: Take the reciprocals. If the reciprocal is ∞ the plane is parallel to that direction. In our case, we obtain the fractional intercepts 1/2, 1, ∞.

Step 2: Multiply the reciprocals with each of the unit cell lengths, a, b and c. By multiplying with a, we obtain a/2, a, ∞.

Step 3: Mark the intercepts and draw the plane (Figure 24).
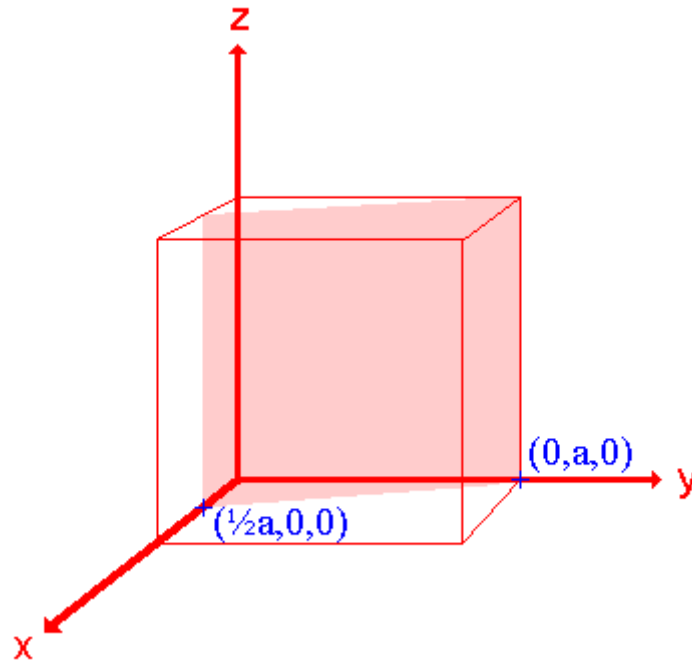
Figure 24: The (210) Miller plane in a cubic structure. [75]

In crystallography the unit cell is not always a cube as we can see in the Bravais lattices section but it can also be a parallelepiped unit cell (at least one of the angles α, β or γ is not 90°), where the lengths (a, b, c) and angles (α, β, γ) between the edge (period) vectors (*a*, *b*, *c*) of the parallelepiped unit cell are known. For simplicity, it is chosen so that edge vector *a* in the positive x-axis direction, edge vector *b* in the x-y plane with positive y-axis component, and edge vector *c* with positive z-axis component in the Cartesian-system, as in Figure 25.
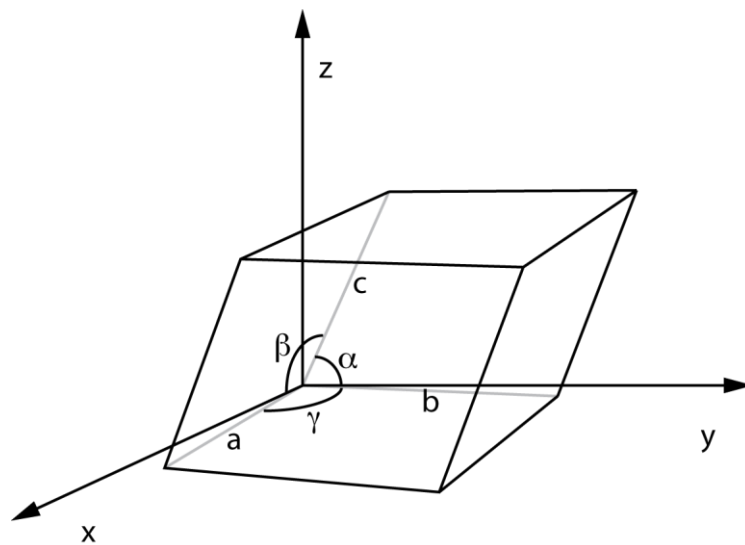
Figure 25: A parallelepiped unit cell (at least one of the angles α, β or γ is not 90o). [76]

Then the edge vectors can be written as:

a = (a, 0, 0),

b = (b*cos(γ), b*sin(γ), 0) and

c = (c_x, c_y, c_z), where:

c_x = c*cos(β),

c_y = c*(cos(α) - cos(β)*cos(γ)) / sin(γ) and

c_z = c*$(1 - \cos^2(α) - \cos^2(β) - \cos^2(γ) + 2*\cos(α)*\cos(β)*\cos(γ))^{1/2}$ / sin(γ)

2.9 Wulff Construction

The Wulff construction is a method to understand and predict the equilibrium shape of nanoparticles [77]. The shape of an equilibrium crystal is obtained, according to the Gibbs thermodynamic principle, by minimizing the total surface free energy associated to the crystal interface showing that specific crystal planes are preferred over others, giving the crystal its characteristic shape [78]. He defined the quantity:

$$\Delta G_i = \sum_j γ_{j}*O_j \quad (3)$$

Where $γ_j$ represents the surface (Gibbs free) energy per unit area of the jth crystal face and Oj is the area of the said face. ΔG_i represents the difference in energy between a real crystal composed of i molecules with a surface and a similar configuration of i molecules located inside an infinitely large crystal. This quantity is, therefore, the energy associated with the surface. The equilibrium shape of the crystal will then be that which minimizes the value of ΔG_i.

Wulff has shown that the distance d of a crystal plane from the origin is proportional to its minimum surface energy γ [79]:

$$d_{hkl} = λ * γ_{hkl} \quad , λ=constant \quad (4)$$

That means that lower surface energy leads to a larger plane area closer to the origin. The Wulff construction results in a polyhedron with the following properties:

- The polyhedron depends only on ratios between surface tensions and not on their absolute values.

- (hkl) planes with high surface tension (usually high-indexed ones) are less likely to appear in the equilibrium shape.

- High-index faces are usually hidden behind low-index ones, even if $γ_{hkl}$ is not very high.

- The extra energy associated with the formation of edges and vertices between two surfaces is neglected.

- Bears the same symmetry (belonging to the same point group) as the crystal structure of the material.
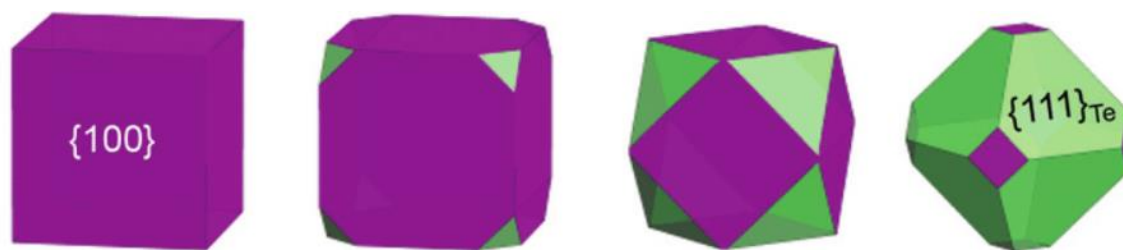
Figure 26: In a crystal shape derived by {100} we slowly decrease the surface energy of {111}, with the latter being the preferred growing plane family in the end. [80]

The growing planes of the crystal, which correspond to its minimum surface energies, can be used to extend the size and shape of the nanoparticle (NP) (Figure 26). These planes are generated by calculations based on the density functional theory (DFT) that calculate the geometries and surface free energies of some surfaces at different compositions, including the stoichiometric plane, and those with a deficiency or excess of oxygen atoms. This method is followed, and Wulff crystal morphology is derived using the lowest surface energies for each Miller index [81].

The Wulff construction offers a rigorous and straightforward way to describe nanoparticle shapes without the need to use complex mathematical language. The shapes can be characterized by two or three parameters (the surface energies of some (hkl) faces and the point group of the material). These parameters can be plugged into a Wulff construction code to reproduce the shape of the nanoparticle.

In the next chapter, the methodology for the construction of the web-based crystallographic tool is presented. As it is already mentioned, individual crystals grow based on their crystal habits, which give the characteristic external shape of a crystal, but crystallographic files contain only the crystal structure and not its crystal shape. The goal of this study is to create a web-based crystallographic tool for the construction of nanoparticles for simulation by building the crystal shape according to the crystal point group and the Wulff morphology and constructing and replicating the symmetric unit cell across all directions according to the crystal space group, inside the crystal shape. A similar process, but not a straightforward one, for constructing crystal shapes and atomic structures can be done by various software programs such as Vesta (which is used to validate the results of this study (chapter 4.2.1)) [82, 83], Mercury [84-87], WinXMorph [88, 89], Materials studio [90] and many others [91], but all of these software programs must be download and installed. Also, some of them are not free, and some others need to download and install additional libraries or software programs. The most significant problem is the use complexity of these software programs as it can become very complicated and challenging to even load a crystal structure let alone the construction of the crystal shape and the nanoparticle.

For that reason, in this study, the first web-based crystallographic tool is created to provide an easily accessible web tool, without installation or sign up, which can produce nanoparticles for simulation from any material as they grow in nature of any type, any size, and any shape.

3. METHODOLOGY

As it was discussed in chapter 1.4, every crystalline material grows with a different crystal habit and different symmetry in nature. By using the crystallographic theory discussed in chapter 2, the crystallographic tool for the construction of nanoparticles (NPs) for simulation was made to provide an easily accessible web-based crystallographic tool, without installation or sign up. The first step was to construct the equilibrium shape of the NP using the Wulff construction (crystal habit) and the second step to fill the equilibrium shape with the crystal atoms by creating and translating the symmetric unit cell, from the asymmetric one, in all spatial directions and as a result the NP Cartesian coordinates are given as output automatically. To facilitate this process, a web service was developed. The algorithm which is described in this chapter was first written in Matlab [92] for visualization purposes and then in the C++ [93] programming language for speed (Figure 27). The web service was coded in PHP [94].

Figure 27: Technologies used for the production of the tool.

3.1 Crystal habit

To construct the crystal habit, which is the first step for the construction of the NP, the following procedure was programmed:

1) Calculate of the symmetric Miller indices and their Miller planes.

2) Find the intersection points of 3 Miller planes for every combination of all the Miller planes and discard those points that fall outside the polyhedron.

3) Create the faces of the polyhedron using the Quickhull algorithm to define the convex hull of a set of points.

As a result, we obtain the equilibrium crystal shape of the NP of any given crystal structure, Miller indices, and size.

3.1.1 Symmetric Miller indices and planes

The first step is to calculate the symmetric Miller indices according to the point group of the crystal structure. These symmetric Miller indices are calculated by multiplying the transpose matrix of the point group with the initial Miller indices which are found from a bibliography or individual quantum mechanical calculations. Then from each one of the symmetric Miller indices, we calculate their Miller planes, as in chapter 2.1.8, to keep a list of the intersecting planes. For each hkl triplet and the desired distance d from the origin that has been provided by the user and is proportional to its minimum surface energy, the xyz coordinates for three points on the miller plane are estimated taking into account the lattice parameters and the fractional coordination system [95]. Next, the coefficients A, B, and C are computed, and the corresponding plane equation P is defined (Figure 28).
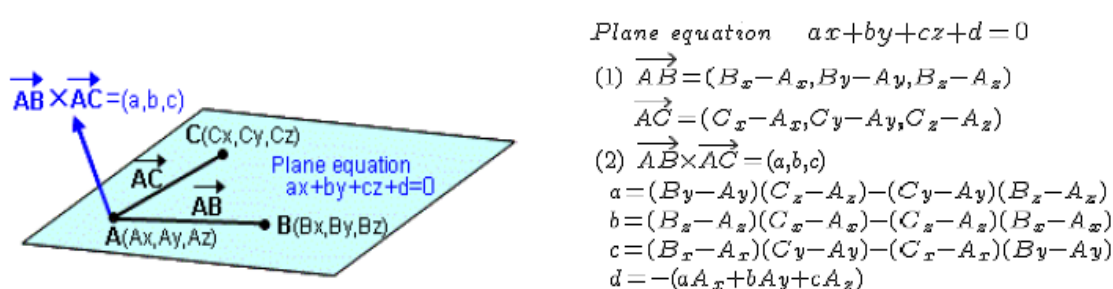
Figure 28: Define the plane equation. [96]

We apply the distance d from the origin provided by the user, and we calculate the coefficient D with the origin to be placed on the negative side (D<0). The last is a convention that is helpful for calculating the vertices of the polyhedron in the next steps.

3.1.2 Intersection points

The next step is the calculation of the polyhedron vertices. To do so, an exhaustive search is performed to find all the intersection points by taking all possible combinations of three planes. For each group of 3 planes, we separate in couples. The intersection of each couple (if nonparallel) is a line, and the intersection of these lines (if nonparallel) is a point (Figure 29).

These points are considered as potential vertices of the polyhedron. The polyhedron is the intersection of multiple polyhedra. Therefore the vertices are the vertices that lie on the "inner" planes (our convention is that the origin [0 0 0] is always on the negative side of all planes). So, the points that fall outside the polyhedron are discarded (it is checked using the plane equations); the rest form the set of the polyhedron vertices V (Figure 30).
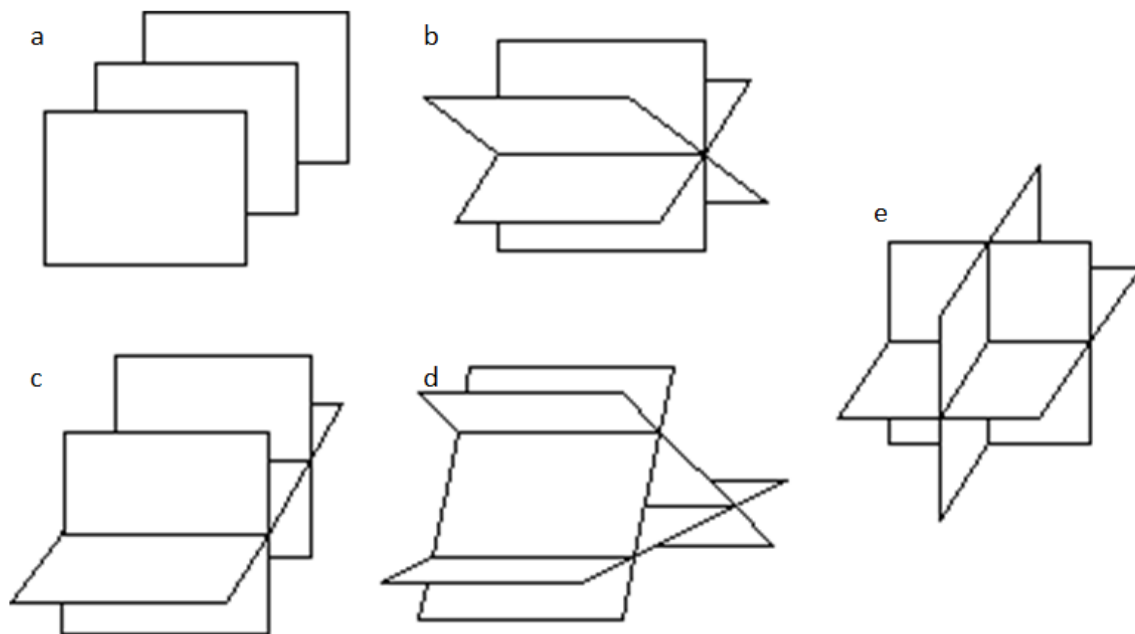
Figure 29: Examples of no intersection point (a, b, c, d) and example of a single intersection point from three planes, each two being non-parallel (e). [97]

Accepted points (-)
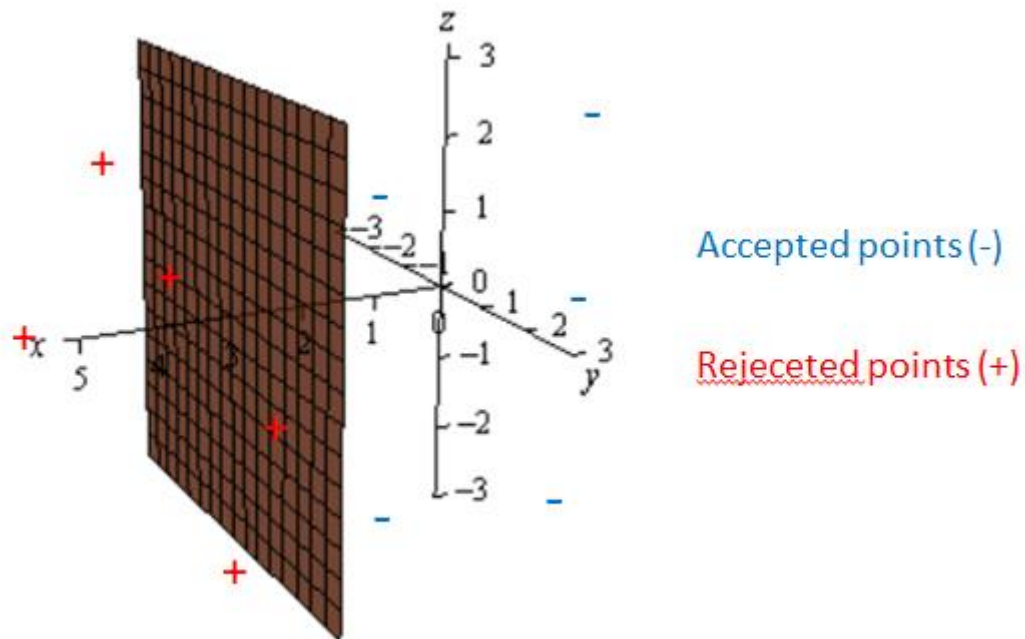
Rejeceted points (+)

Figure 30: Calculating polyhedron vertices (rejected and accepted points). [98]

3.1.3 Polyhedron faces

The third step is the definition of the polyhedron faces. In principle, we note that each face is a polygon that lies on one of the planes, it is defined by a subset of V and by a set E of ordered edges, i.e., line segments that connect vertices. For each plane, all

vertices that lie on it (satisfies the plane equation) are first defined. The vertices are arranged sequentially so that the line segments that constitute the edges of the polygon are indicated. Then, a polygon is created given these vertices using the Quickhull algorithm [99]. With the Quickhull algorithm, the convex hull of a set of points (in our case, the subset of the vertices) is defined.

The convex hull of a geometric object (such as a point set or a polygon) is the smallest convex set containing that object (Figure 31). There are many equivalent definitions for a convex set S. The most basic of these is that a set S is convex if whenever two points P and Q are inside S and then the whole line segment PG is also in S.
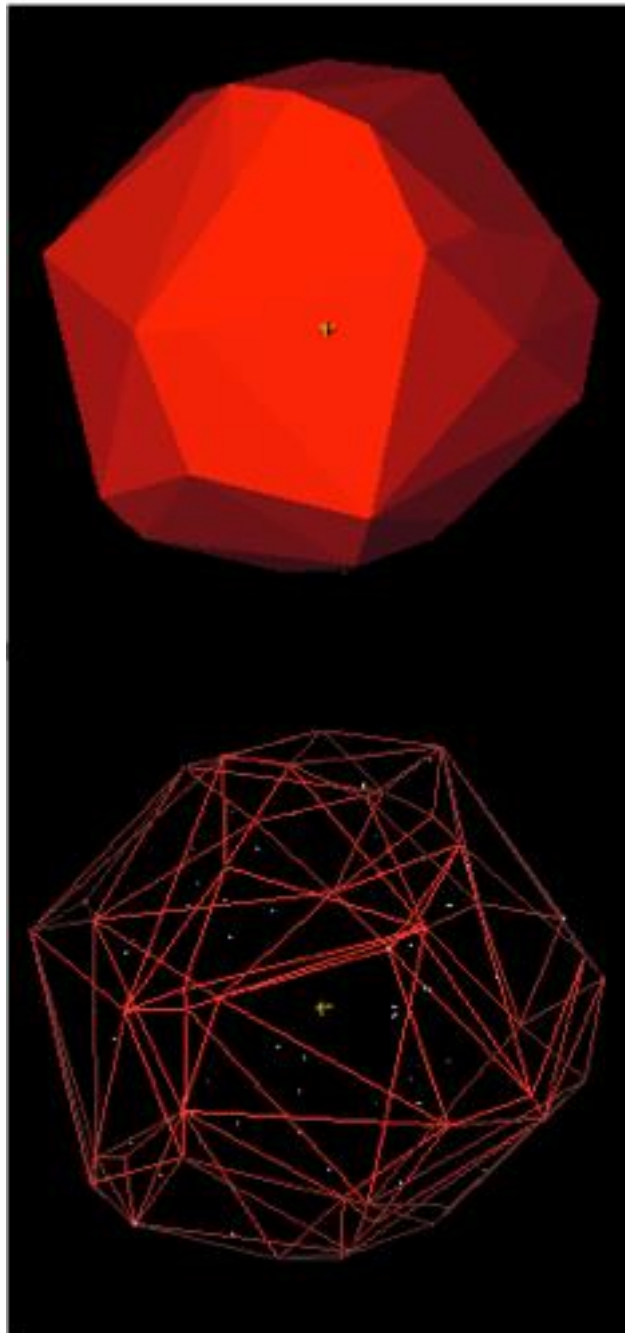
Figure 31: The 3D convex hull of 120 point cloud. [100]

The Quickhull algorithm uses the divide and conquer approach, and its average case complexity is considered to be O(n*log(n)), whereas in the worst case it takes O(n2). In our implementation of the algorithm, the most distant points are connected with a (double) line segment, which initializes the set E. Then, in each of the iterative steps, the most distant point from any of the line segments in E is found; that line segment is replaced with two new ones, connecting the most distant point. The iterative steps of the algorithm stop when all points have been included in the convex hull (Figure 32). This way, for each plane we obtain an ordering of the edges that form a closed chain.
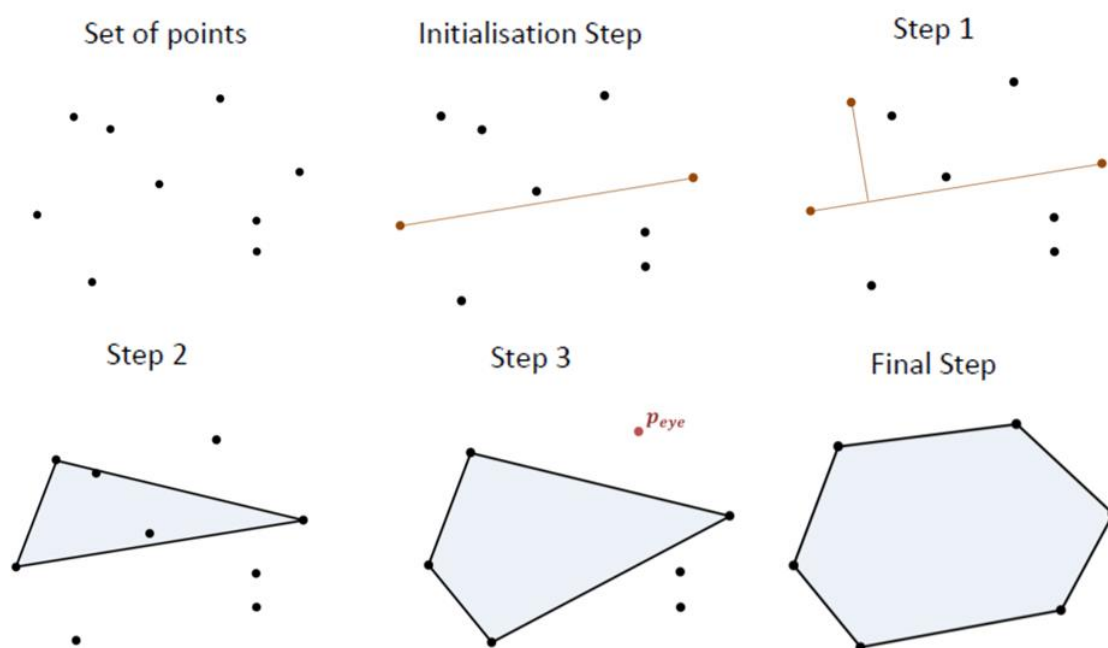
Figure 32: Quickhull algorithm steps. [101]

So with the preferred growing planes of the crystal in Miller indices, their corresponding minimum surface energies (Wulff construction) and the desired maximum radius that the user wants we can build the equilibrium shape (Wulff morphology) of any crystal of any space groups, lattice parameters, and size (Figure 33).

Figure 33: The workflow for the construction of the Wulff morphology.

3.2 Unit cell replication

Now that we have the shape of the nanoparticle the next step is to fill that shape with the crystal atoms. To do that we have to:

1) Build the symmetric unit cell from the asymmetric one.

2) Replicate the symmetric unit cell in all three spatial directions until the equilibrium shape is filled.

As a result, we will obtain the final nanoparticle with the Cartesian coordinates of all atoms.

3.2.1 Symmetric unit cell

The first step to fill the equilibrium shape with atoms is to calculate the symmetric unit cell from the asymmetric one. The asymmetric unit refers to the smallest possible occupation of space within the unit cell. The atom positions within the unit cell can be calculated by applying the symmetry operations to the asymmetric unit (Figure 34). This procedure, however, does not imply that the entirety of the asymmetric unit must lie within the boundaries of the unit cell [102]. Symmetric transformations of atom positions are calculated from the space group of the crystal structure which can be found in the crystallographic file of the crystal structure (cif), which contains all the required information of a crystal, such as the crystal parameters, the symmetry operations of the crystal space group and the Cartesian coordinates of the atoms as fractions of the unit cell length values [103]. The algorithm that is applied to build the symmetric unit cell from the asymmetric one is:

- Step 1: Apply the given symmetry operations (obtained from the crystallographic file) to the atoms of the asymmetric unit and remove duplicated atoms. As a result, a list of atoms is obtained with their Cartesian coordinates (Figure 35).

- Step 2: Atoms that are outside the asymmetric unit cell should be moved inside. The asymmetric unit cell is a cube with lengths of 1 angstrom with the origin being on the bottom left edge. So if one of the Cartesian coordinates of the atom is below 0 or over 1, we add or subtract 1 respectively.

- Step 3: Atoms that are on the unit cell faces should be copied to its parallel face.

- Step 4: Atoms that are on an edge should be copied to all edges.

- Step 5: Apply the lattice parameters on atom coordinates.

As a result of this methodology, we obtain the final symmetric unit cell of the crystal (Figure 36). In Figures 34-36 there is an example of this methodology for the TiO2 crystal structure.
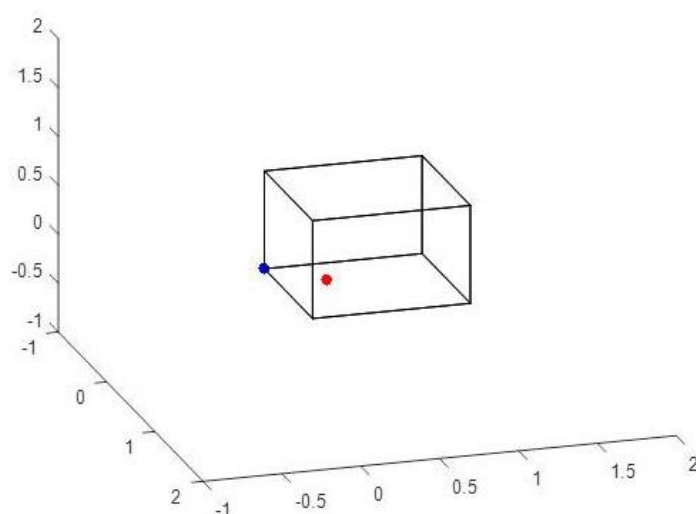
Figure 34: Example of the asymmetric unit cell of the TiO2 (with blue the Ti atom and with red the O atom).
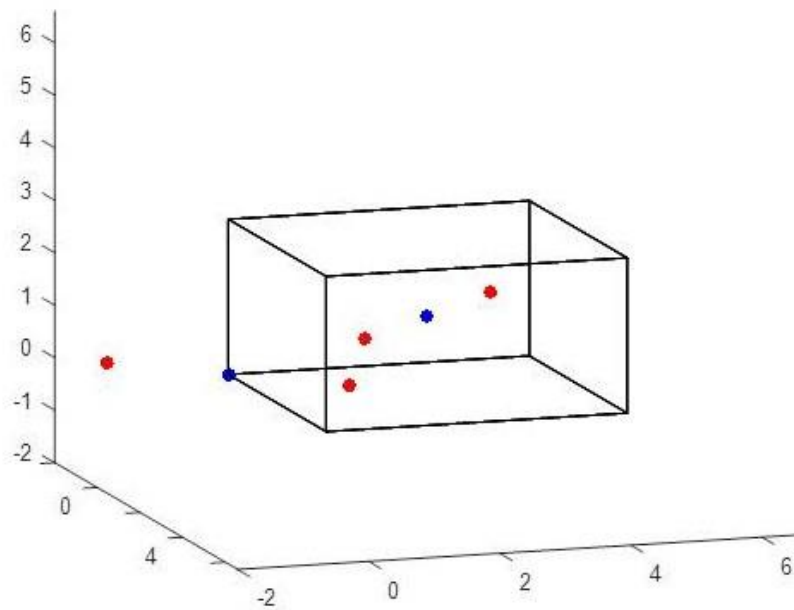
Figure 35: Example of the asymmetric unit cell of the TiO2 after the symmetry operations are applied (with blue the Ti atoms and with red the O atoms).
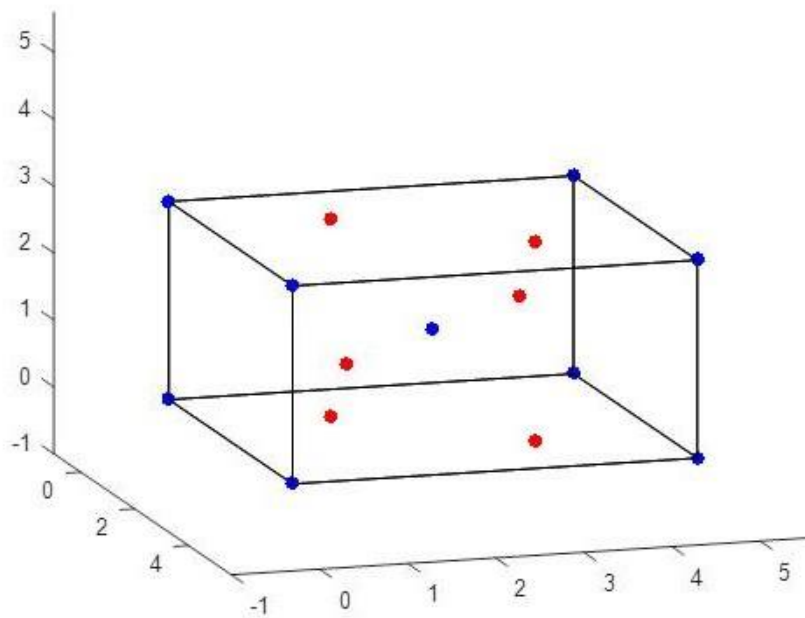
Figure 36: Example of the final symmetric unit cell of the TiO2 unit cell (with blue the Ti atoms and with red the O atoms).

3.2.2 Replication of unit cell

The second step in order to fill the equilibrium shape with atoms is to replicate the symmetric unit cell of the previous stem along all three spatial directions until the equilibrium shape is filled. The algorithm that is applied to do that is:

- Step 1: Replicate the symmetric unit cell across all directions as until it reaches the maximum length of x, y, and z of its equilibrium shape (constructed from the methodology followed in chapter 2.2.1 (Figure 38). As a result, a big cube or parallelepiped is built (Figure 37).

- Step 2: Remove duplicated atoms.

- Step 3: Remove atoms that are outside the equilibrium shape, or else remove atoms that are on the positive side of at least one of the planes, the same way the intersection points were rejected in chapter 2.2.1.2.

As a result of these steps (Figure 40), the final nanoparticle is constructed (Figure 39), and a list of all the atoms and their Cartesian coordinates are produced.
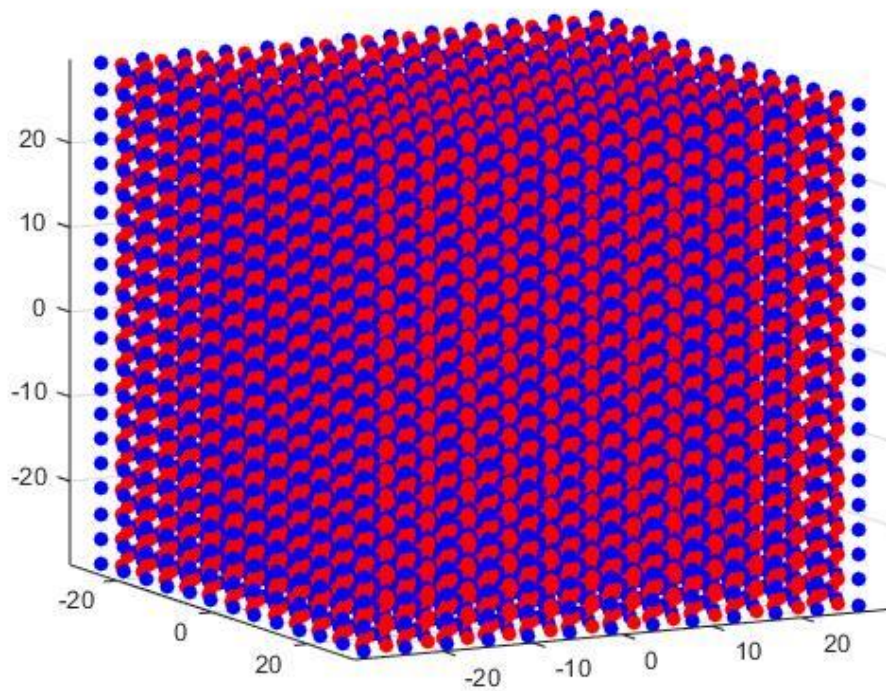
Figure 37: Example of the product of the TiO2 unit cell replication across all directions until the maximum lengths of x, y and z of its equilibrium shape are reached (with blue the Ti atoms and with red the O atoms).
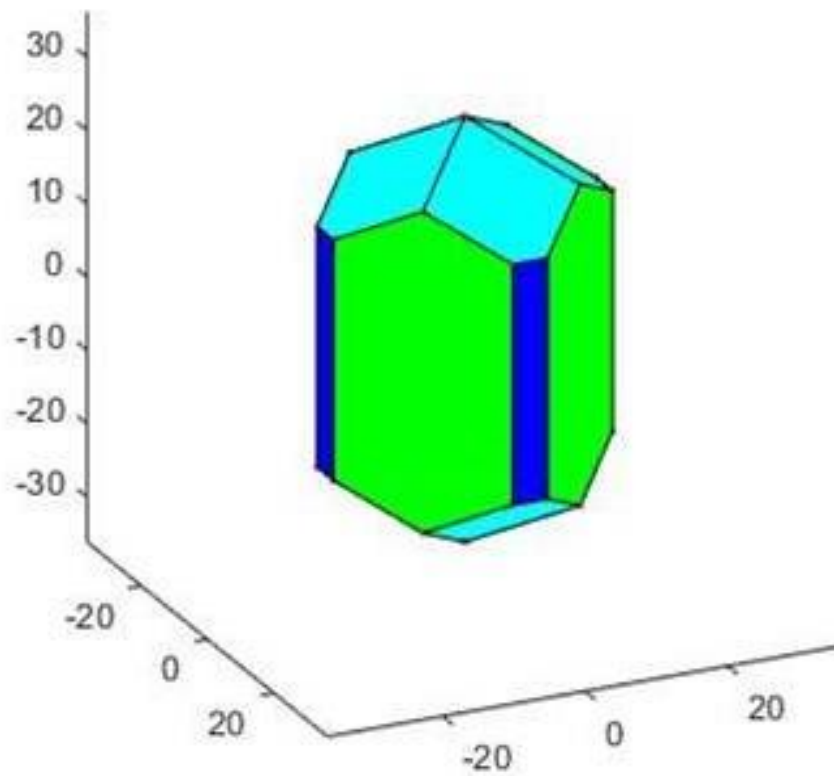
Figure 38: Example of the TiO2 equilibrium shape (with blue the Ti atoms and with red the O atoms).
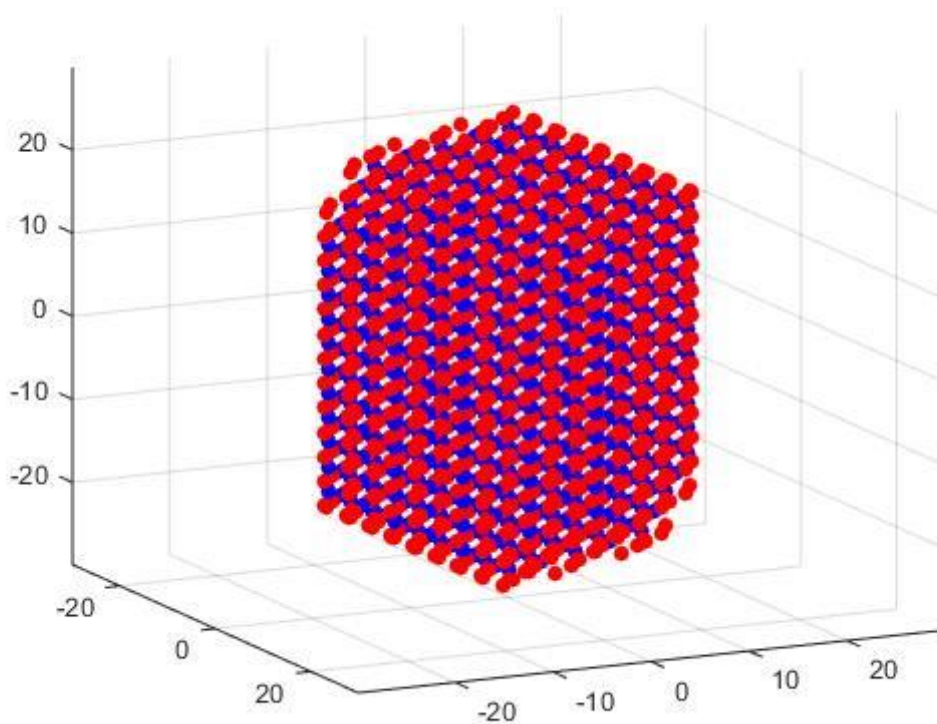
Figure 39: Example of the final TiO2 nanoparticle (with blue the Ti atoms and with red the O atoms).
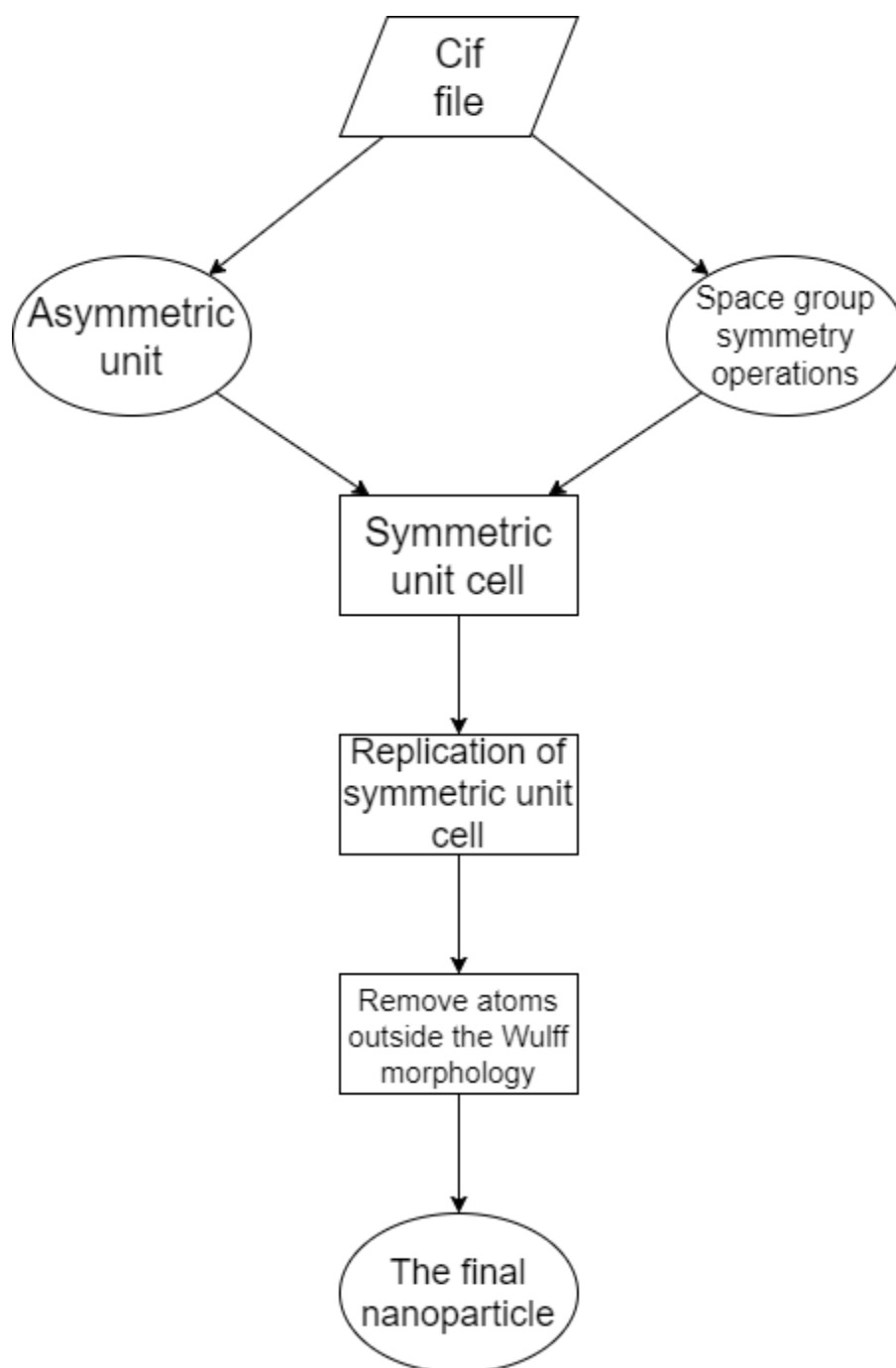
Figure 40: The workflow for the construction and replication of the symmetric unit cell and the construction of the final nanoparticle

3.3 Web development

In the previous chapter, the methodology and the algorithm for the construction of nanoparticles for modeling were analyzed. The tool was developed using the C++ programming language, and the next step is to create a website which will make the tool easily accessible for the users, without installation and account creation.

This work was done using PHP (Hypertext Preprocessor), which is a widely-used, free, and efficient server scripting language, and a powerful tool for making dynamic and interactive web pages [94] (Figure 41).

Figure 41: The PHP programming language used to create the website.

Using PHP the site downloads the cif file input, which can be found from http://crystallography.net/ [104-108], and also writes the Miller indices and the corresponding minimum surface energies, which can be found from literature or quantum mechanical calculations, into a text file for the C++ code to read them. Then again using PHP the site uploads the produced xyz and pdb files to the user. Lastly in the same way the user can download the example which is on the site and also read the manual (Annex I), to help users understand how to use the tool.

In addition to the previous PHP code, of course HTML (Hypertext Markup Language) [109], CSS (Cascading Style Sheets) [110] and JavaScript [111] codes were implemented. Also, the JQuery, a cross-platform JavaScript library, as well as other JavaScript libraries and JavaScript code were also used and programmed. The JSmol was also added, which is a fully functional implementation of Jmol that does not require Java and runs in any modern (HTML5) web browser [112, 113] (Figure 42). Jmol is an open-source viewer for three-dimensional chemical structures, with features for chemicals, crystals, materials, and biomolecules, which visualizes the produced nanoparticle.

Figure 42: An open-source viewer for the nanoparticles.

4. RESULTS

In this chapter, the program use, and some use cases are presented. In the program use subchapter, there are analytically the required inputs of the web application, the implementation of the algorithm which is presented in the first subchapter and the output of this crystallographic tool. Then some use cases are explored for a better understanding of the tool along with the validation of the results.

4.1 Program use

As it is already said, this tool constructs nanoparticles for simulation. The required inputs are explored as well as the back-end implementation of the algorithm, although the latter is not required knowledge for the user. At last, the output is explored and the visualization process.

4.1.1 Inputs

The first input is the crystal structure given as a .cif, which is the crystallographic file found in the www.crystallography.net, which contain all the information of the crystal such as its crystal parameters, its point group, its space group, the atomic Cartesian coordinates of the asymmetric unit cell, etc. (Figure 43).
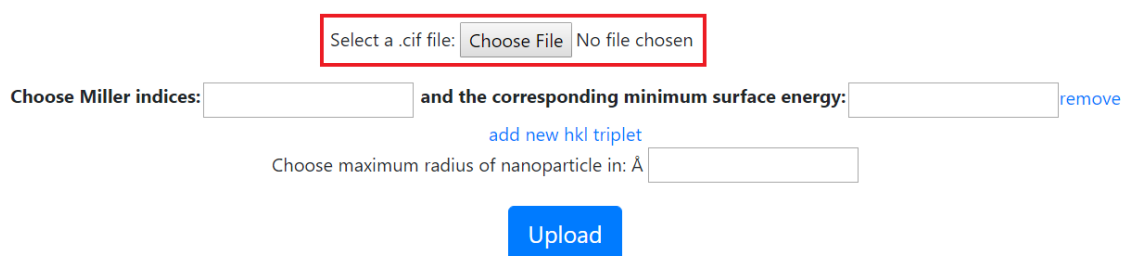
Figure 43: The first input which is the .cif file.

The next inputs are the Miller indices and their corresponding minimum surface energies (Figure 44), which can be found either from a bibliography or your quantum mechanical calculations based on the Wulff construction. These energies can be in any units (but the same between them) because the Wulff construction results in a polyhedron that depends only on ratios between surface tensions and not on their absolute values.

Figure 44: The next inputs.

There is an option to add many hkl triplets along with their minimum surface energies and an option to delete in case that false input is added (Figure 45).

Figure 45: Options to add or remove inputs.

For example, the user can put three hkl triplets and minimum surface energies as it is shown in Figure 46.

Figure 46: Multiple inputs (Miller indices and energies).

The final input is the maximum radius of the nanoparticle in Angstroms which determines the size of the nanoparticle the user wants (Figure 47).

Figure 47: The final input (maximum radius of the NP).

4.1.2 Implementation of the algorithm

After pressing the upload button, the tool produces the symmetric Miller indices for each hkl triplet input, according to the point group of the crystal, which is taken from the crystallographic file. As a result, a list of all symmetric Miller indices is obtained. From each one of the hkl triplet in this list, three Cartesian coordinates are produced from the fractional coordinates and the unit cell's parameters as it is already shown in chapter 2.1.8, which are enough to produce a plane. So, from the list of Miller indices, we obtain a list of the corresponding Miller planes. These planes are placed at a distance from the origin, which is proportional to their surface energy and the maximum radius the user inputted.

Then the tool finds the intersection points for all three combinations of these Miller planes and discards those that lie outside of at least one plane. Then the tool matches the Miller planes with the intersection points that lie on them, or else the points that satisfy the plane equations. As a result, the faces of the equilibrium shape are obtained and using the Quickhull algorithm the equilibrium shape is constructed.

Lastly, from the crystallographic file, the tool takes the atoms of the asymmetric unit cell, the crystal parameters and the symmetry operations of the crystal's space group. These symmetry operations and crystal parameters are applied to the atoms of the asymmetric unit cell, which gives symmetric unit cell and its atoms. The symmetric unit cell is then translated along all three spatial directions until the maximum length of the equilibrium shape is reached, forming a cube with atoms. At last, we keep those atoms that are inside the equilibrium shape (Wulff morphology), and the nanoparticle is built. In Figure 48 the workflow of the above procedure is shown.
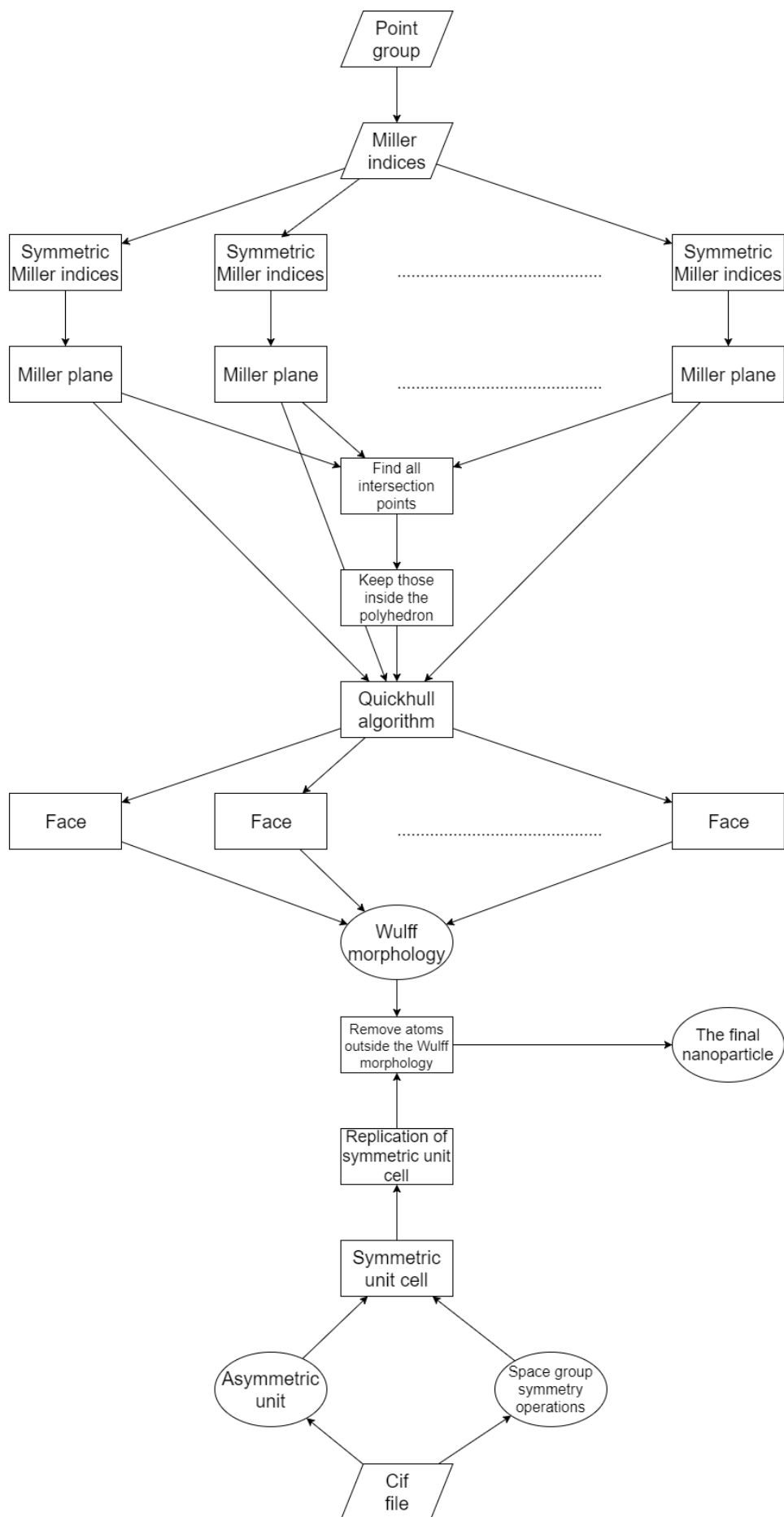
Figure 48: The workflow for the construction of nanoparticles for simulation.

4.1.3 Output

As a result, the user has the choice to download the coordinates of the atoms in a .xyz file and a .pdb file and also visualize the nanoparticle using the Jsmol plugin. Also, there is a return button in case the user wants to construct another nanoparticle for simulation (Figure 49).
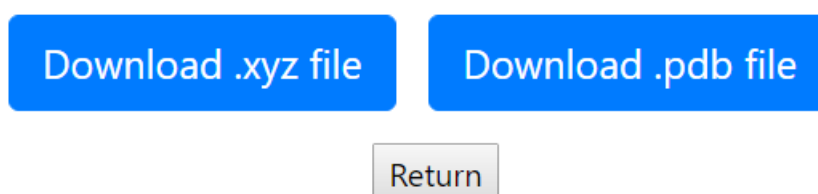
Figure 49: The download options.

4.2   Use cases

In this chapter, some use cases are shown in order to have a better understanding of the tool, such as the construction of the Fe3O4 (magnetite) NP, the TiO2 rutile NP, and the LiFePO4 NP along with their validation. The equilibrium shapes are visualized in Matlab and the final nanoparticles with the JSmol.

4.2.1 Validation

All of the examples were also produced for validation purposes using the Vesta tool, which is a 3D visualization program for structural models, volumetric data such as electron/nuclear densities, and crystal morphologies with many novel features [82, 83] (Figure 50). Keep in mind that Vesta puts an extra layer of atoms after the maximum size of the nanoparticle is reached.

Figure 50: The tool used to validate the results.

4.2.2 Use case 1, Fe3O4

The first input as it is already said is the cif file of the crystal. The magnetite's (Fe3O4) crystallographic file can be acquired and downloaded from http://crystallography.net/cod/9010940.html [114]. The magnetite is a cubic crystal structure with unit cell lengths a=b=c=8.3198 angstroms and cell angles α=β=γ=90°. In the magnetite's cif file also the symmetry operations and the Cartesian coordinates of the atoms of the asymmetric unit can be found. The Miller indices and minimum surface energies are found from bibliography [115], where the density factional theory (DFT) was used (Table 1). In literature also the (011) surface was studied but despite having a surface energy of the same order of magnitude as the others, it is not expressed in the Wulff construction due to competition with the (001) surface, so it was not in the inputs of this example.

Table 1: The Fe3O4 Miller indices and minimum surface energies.

Miller indices	Energies (J/m^2)
001	0.96
111	1.09

The user chooses the last input which is the maximum radius of the NP and in this example, we choose 30 angstroms.

The tool then follows the algorithm which is already discussed and produces 14 symmetric hkl triplets from the (001) and (111) Miller indices. Then the 14 Miller planes are generated from these hkl triplets using the Wulff construction by placing the Miller planes of the {111} family in a distance of 30 angstroms from the origin and the Miller planes of the {001} family in a distance of 26.422 angstroms from the origin. These planes have 24 accepted intersection points, which along with the 14 Miller planes give the 14 faces of the equilibrium shape. Then using the Quickhull algorithm the equilibrium shape is produced (Figure 51 (a)).
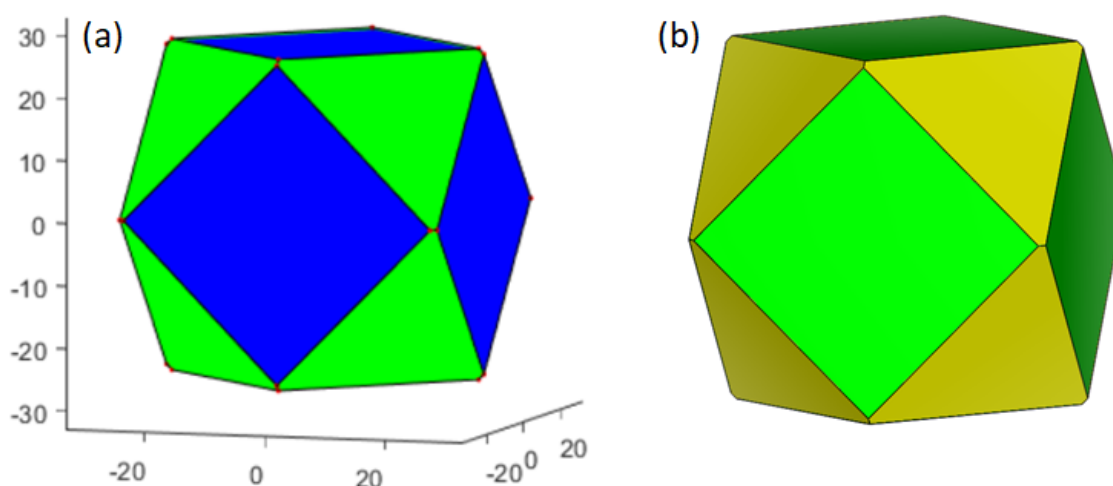
Figure 51: The equilibrium shape of the Fe3O4 NP produced in Matlab (a) and Vesta (b).

Then the tool produces the symmetric unit cell the way it was discussed in chapter 2.2.2.1 and translates it across all directions until the above equilibrium shape is filled. As a result, the Fe3O4 nanoparticle is produced (Figure 52 (a)).
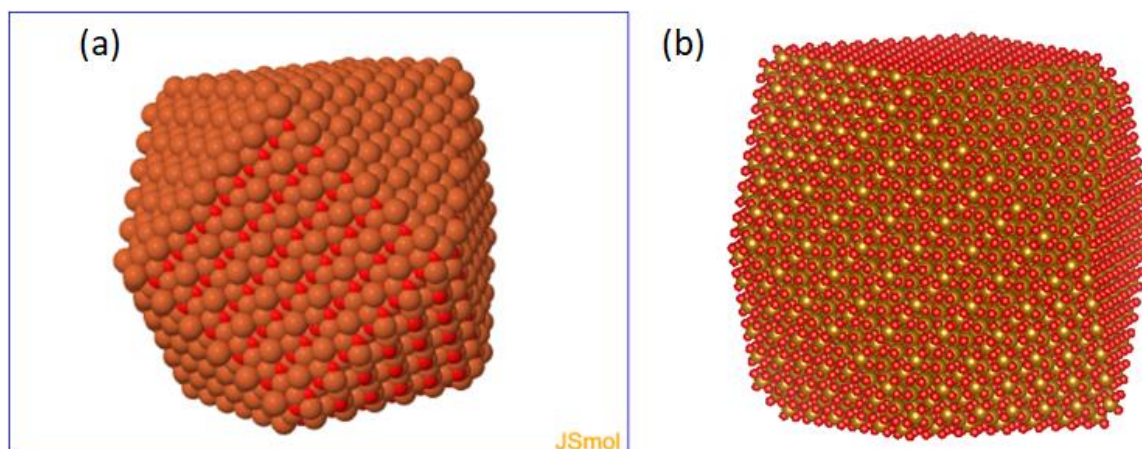
Figure 52: The Fe3O4 NP visualized using JSmol (a) and Vesta (b).

The coordinates of the atoms are downloaded in a .pdb and a .xyz format. The total size of the atoms is 11.222 (Figure 53).

Figure 53: Fragment of the resulted magnetite atom coordinates in .xyz and .pdb formats.

The magnetite NP with a maximum radius of 15 angstroms was also modeled to perform atomistic MD simulations to assess the interactions between two functionalized nanoparticles and the DPPC lipid bilayer in atomic-level detail. For functionalizing the magnetite core, polyvinyl alcohol (PVA) and polyarabic acid (ARA) were used. Quantification of the MD trajectory, by means of radial distribution function and mean square displacement, showed that both NPs interact strongly with the DPPC lipid bilayer, indicating that the magnetite-PVA nanoparticle may interact more strongly with the model membrane.

4.2.3 Use case 2, TiO2

For the TiO2 rutile example, the crystallographic file can be downloaded from http://crystallography.net/cod/9009083.html [116]. The TiO2 rutile is a tetragonal crystal structure with unit cell lengths a=b=4.59373 and c=2.95812 angstroms and cell angles α=β=γ=90°. In the TiO2 rutile's cif file also the symmetry operations and the Cartesian coordinates of the atoms of the asymmetric unit can be found as in the previous example. The Miller indices and minimum surface energies again are found from bibliography [117] (Table 2). The (001) surface is barely visible in the Wulff shape, but it is input in this example.

Table 2: The TiO2 rutile Miller indices and minimum surface energies.

Miller indices	Energies (J/m^2)
110	15.6
100	19.6
011	24.4
001	28.9

For this example, we choose 15 angstroms for the last input which is the maximum radius of the NP.

From these Miller indices, the tool produces a total of 18 unique symmetric hkl triplets. Then the 18 Miller planes are generated from these hkl triplets using the Wulff construction by placing the Miller planes of the {110} family at a distance of 8.097 angstroms from the origin, the Miller planes of the {100} family at a distance of 10.173 angstroms from the origin, the Miller planes of the {011} family at a distance of 12.664 angstroms from the origin and the Miller planes of the {001} family at a distance of 15 angstroms from the origin. These planes have 32 accepted intersection points, which along with the 18 Miller planes give the 18 faces of the equilibrium shape. Then using the Quickhull algorithm the equilibrium shape is produced (Figure 54 (a)).
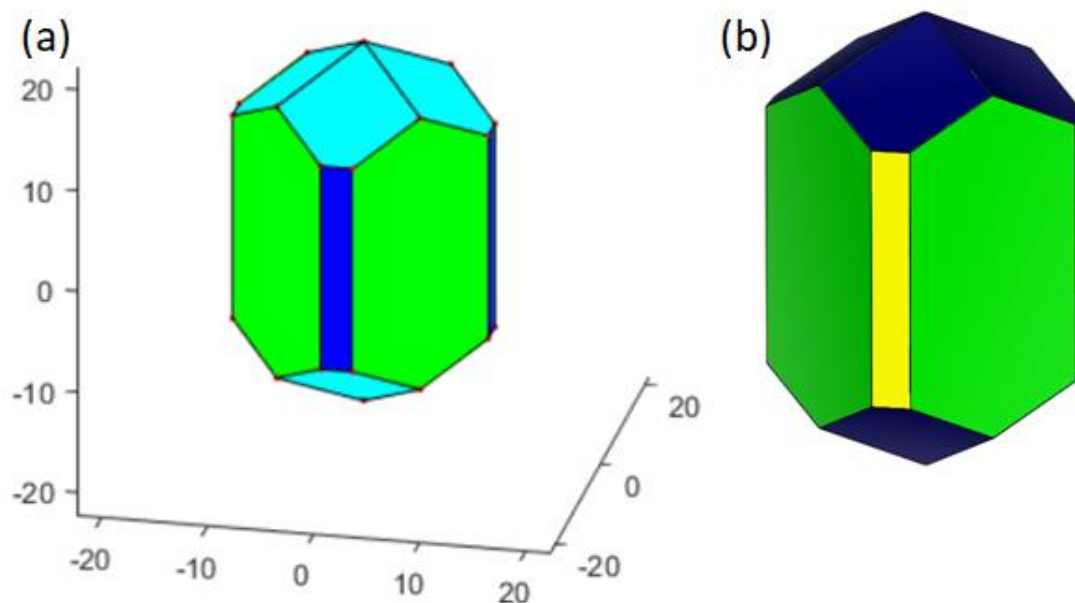
Figure 54: The equilibrium shape of the TiO2 rutile NP produced in Matlab (a) and Vesta (b).

Then the tool produces the symmetric unit cell the way it was discussed in chapter 2.2.2.1 and translates it across all directions until the above equilibrium shape is filled. As a result, the TiO2 rutile nanoparticle is produced (Figure 55 (a)).

Figure 55: The TiO2 rutile NP visualized using JSmol (a) and Vesta (b).

The coordinates of the atoms are downloaded in a .pdb and a .xyz format. The total size of the atoms is 595 (Figure 56).

Figure 56: Fragment of the resulted TiO2 rutile atom coordinates in .xyz and .pdb formats.

4.2.4 Use case 3, LiFePO4

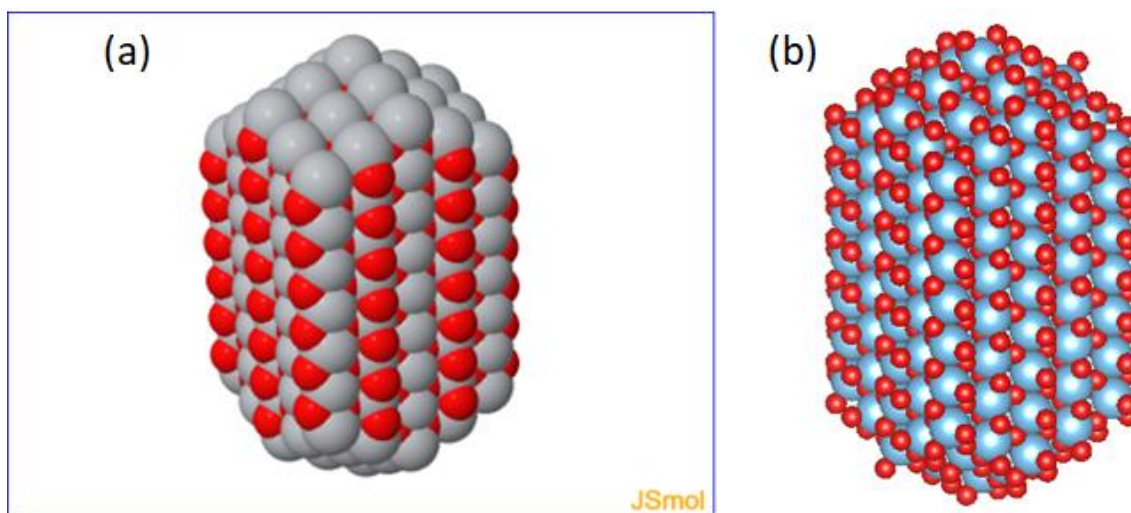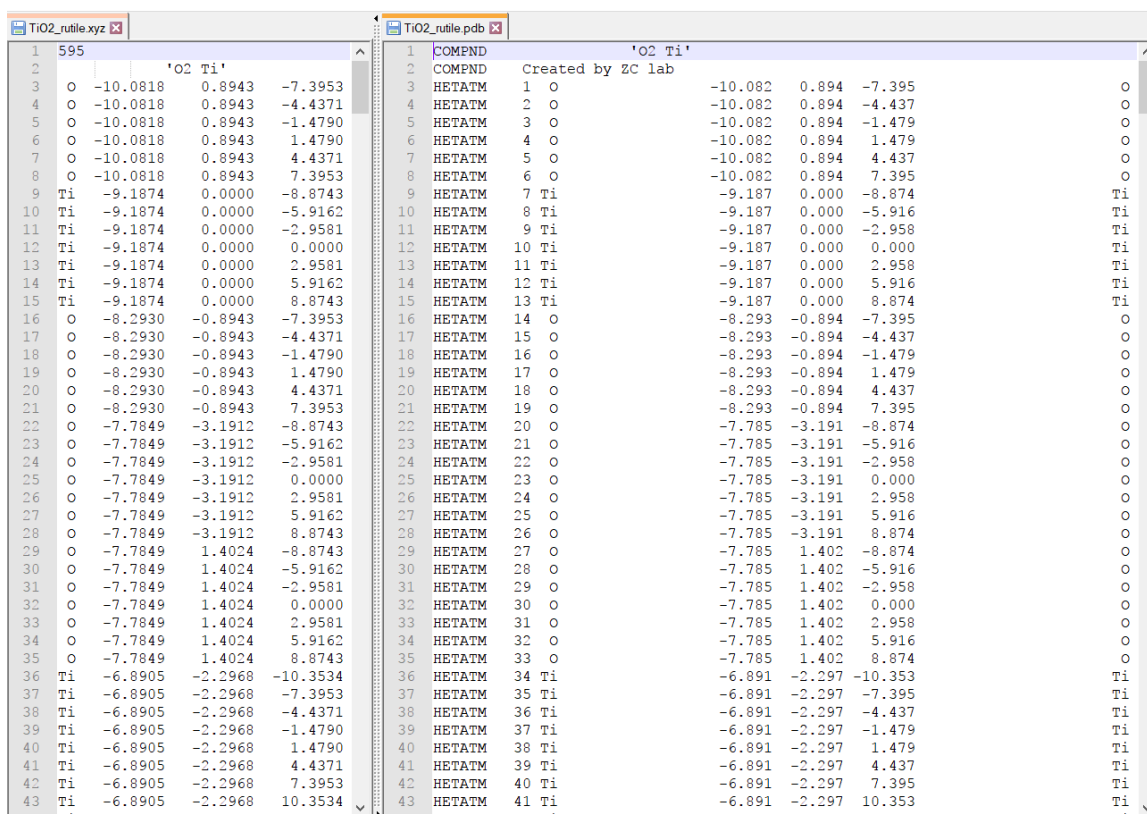For the LiFePO4 example, the crystallographic file can be downloaded from http://www.crystallography.net/cod/4001845.html [118]. The LiFePO4 is an orthorhombic crystal structure with unit cell lengths a=10.336, b=6.006 and c=4.6932 angstroms and cell angles $\alpha=\beta=\gamma=90^o$. In the LiFePO4's cif file also the symmetry operations and the Cartesian coordinates of the atoms of the asymmetric unit can be found as in the previous examples. The Miller indices and minimum surface energies again are found from bibliography [119] (Table 3). In literature 9 Miller indices were studied, but 4 of them do not appear, so they were discarded in this example.

Table 3: The LiFePO4 Miller indices and minimum surface energies.

Miller indices	Energies (J/m^2)
100	0.66
010	0.64
101	0.62
011	0.76
201	0.52

For this example, we choose to build a slightly large nanoparticle with a maximum radius of 50 angstroms.

From these Miller indices, the tool produces a total of 16 unique symmetric hkl triplets. Then the 16 Miller planes are generated from these hkl triplets using the Wulff construction by placing the Miller planes of the {100} family at a distance of 43.421 angstroms from the origin, the Miller planes of the {010} family at a distance of 42.105 angstroms from the origin, the Miller planes of the {101} family at a distance of 40.789 angstroms from the origin, the Miller planes of the {011} family at a distance of 50 angstroms from the origin and the Miller planes of the {201} family at a distance of 34.211 angstroms from the origin. These planes have 24 accepted intersection points, which along with the 16 Miller planes give the 16 faces of the equilibrium shape. Then using the Quickhull algorithm the equilibrium shape is produced (Figure 57 (a)).
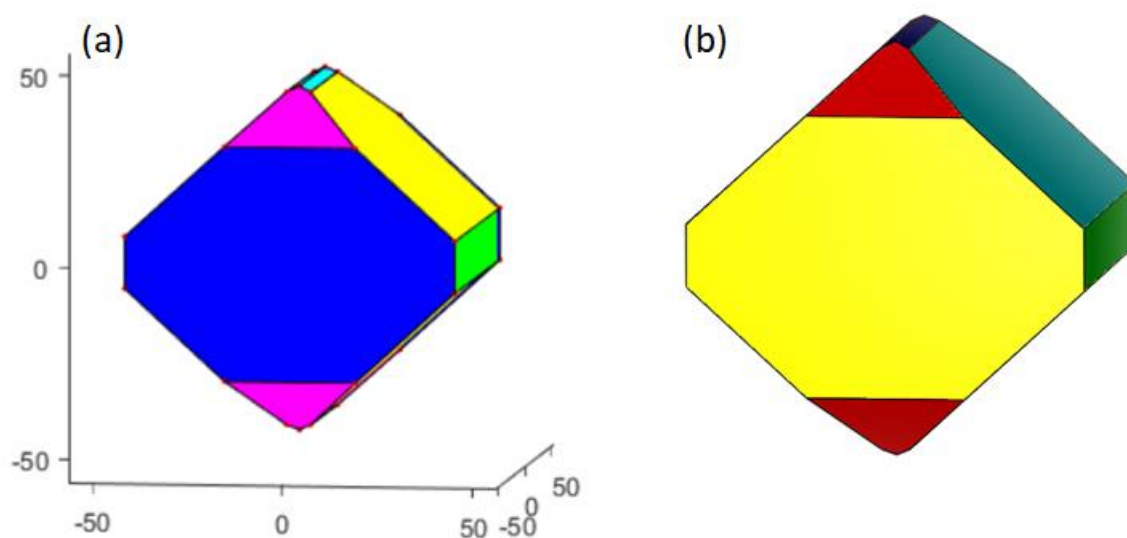
Figure 57: The equilibrium shape of the LiFePO4 NP produced in Matlab (a) and Vesta (b).

Then the tool produces the symmetric unit cell the way it was discussed in chapter 2.2.2.1 and translates it across all directions until the above equilibrium shape is filled. As a result, the LiFePO4 nanoparticle is produced (Figure 58 (a)).
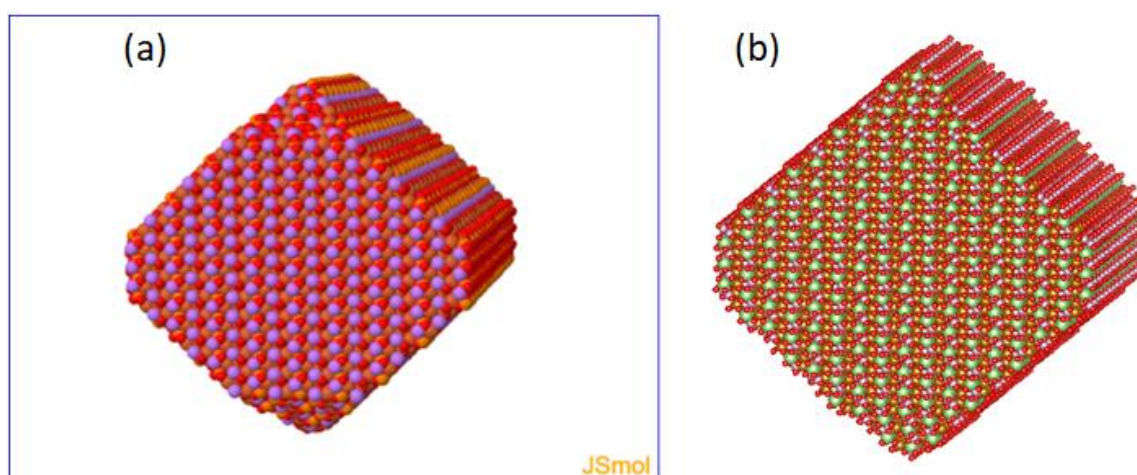
Figure 58: The LiFePO4 NP visualized using JSmol (a) and Vesta (b).

The coordinates of the atoms are downloaded in a .pdb and a .xyz format. The total size of the atoms is 36.355 (Figure 59).

Figure 59: Fragment of the resulted LiFePO4 atom coordinates in .xyz and .pdb formats.

CONCLUSIONS

In recent years, nanotechnology has attracted significant interest in many industrial domains as well as from scientists and engineers of nearly all disciplines. Building a nanoparticle (NP) for simulation it is not an easy task, and it can be very a tedious task. The existing crystallographic files only contain the crystal structure but not the crystal shape, and that gave the motivation to construct this tool to help the interested in nanotechnology to quickly make the nanoparticle they want for simulation.

In this study, the biological background of the system of interest is introduced. The importance of nanoparticles is introduced and some of their applications in various domains. The crystallographic theory is also presented including the unit cell, the crystal systems, the centering types, the Bravais lattices, the crystallographic point groups, the crystallographic space groups, the Miller indices along with the fractional coordination system and the Wulff construction.

In the last decades, significant efforts have been made to predict precisely the growth morphology of crystals. However, it is still a challenging task. Crystals reveal a large variety of shapes, depending on the chemical composition, their structure, and the growth conditions. The shape of the crystals has a direct impact on the separation efficiency and the stability of crystalline chemicals, the bioavailability and the effective delivery of drugs [120]. The knowledge of the growth habits and morphological properties of the molecular crystals is of crucial importance in understanding and exploiting many of their physicochemical properties.

At first, an algorithm was implemented that constructs different morphologies for a given crystal based on its preferred growing planes in Miller indices and their corresponding surface energies and a user-defined size of the crystal (crystal habit). That crystal is a polyhedron that is created as the intersection of multiple polyhedra and individual planes. The next step was to expand this algorithm to find the coordinates of the atoms in extreme precise that lies inside the previously constructed polyhedron. As a result, the final nanoparticle is constructed, and the coordinates of the atoms are served in xyz and pdb files and also visualized to the user thru the website. All of the results in the validation process are in agreement with the ones produced from Vesta. The website can be reached at the following address:

http://nanocrystal.vi-seem.eu/CrystalTool

FUTURE PERSPECTIVES

This tool can be the groundwork for a bigger application which can be even more automated or do some further simulation and prediction after the nanoparticle is built.

One process that can be induced within our web server is to apply the Donnay-Harker principles to calculate each crystal habit [121]. Donnay and Harker refined this approach by developing rules that use the crystal lattice and space group symmetry to generate a list of possible growth faces. These rules account for the effect of translational symmetry operators, meaning that higher-order planes can grow in preference to lower-order ones. Any face forbidden by the symmetry (Donnay Harker) has its indices increased as necessary, for example, (200) face may replace (100). That would make the tool more automated giving a choice for users to put fewer inputs, so they do not have to find the crystal habit from the literature or by making their quantum chemical calculations.

The resulted crystal morphology from the Donnay-Harker rules is an approximation based only on crystallographic geometrical considerations, which means that no energy consideration has been made in this model [122-124]. As a result, the predicted morphology often does not correspond to the experimental observations. Another way to find the crystal morphology is the Hartman-Perdok method, which represents a great improvement that takes into account the energy of deposition of growth units on a pre-existing crystal face. In the Hartman-Perdok theory, it is proposed that the higher the attachment energy of a given (hkl) face, the less the morphological importance of this face in the growth form.

There is also a third method for calculating the crystal morphology by using the Ising model where a real crystal system can be determined by [125]:

i.   Identifying the strong bonds in the crystal structure and calculating their relative bond strengths.

ii. Derivation of the connected nets of the important crystallographic forms.

iii. Conversion of the connected nets into rectangular nets.

iv. The use of the bond energies and rectangular nets to calculate the critical temperature θ^c.

v.   The use of the reciprocal of these values to compute the theoretical morphology.

The Ising model reflects the stable crystal morphology close to the growth conditions for kinetic roughening (i.e., at the transition from a smooth to a rough interface). Thus it should be considered to be a 'stability' model [126]. In Figure 60 there is a scheme showing the previous three methods for calculating the crystal morphology.

This tool can also be expanded by putting ligands on the surface of the constructed nanoparticle for biomedical applications. For example, as it is already shown in chapter 3.3.2 by attaching polyvinyl alcohol (PVA) and polyarabic acid (ARA) on the surface of the magnetite (Fe_3O_4) nanoparticle for cancer treatment (Figure 61).
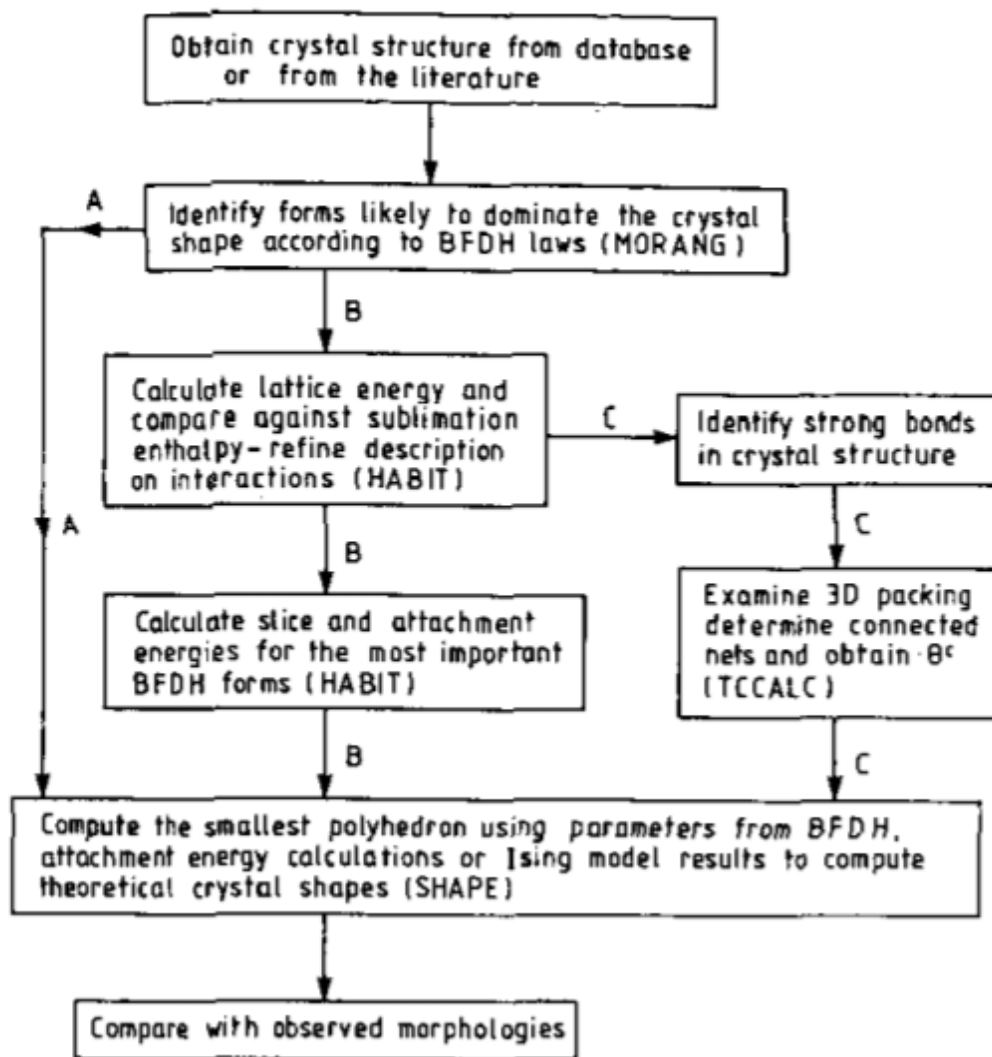
Figure 60: Schematic showing the basic approach for carrying out morphological calculations. Path A produces model the Donnay-Harker model, path B the Hartman-Perdok model and path C the Ising method. [126]
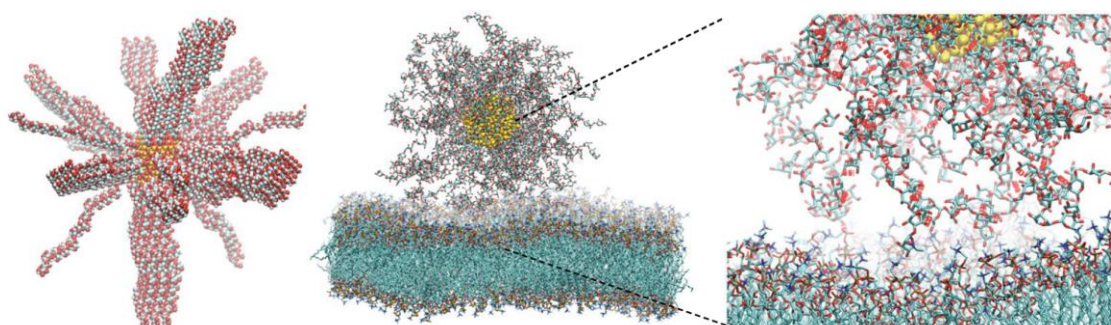
Figure 61: Membrane interaction of a magnetic nanoparticle coated with polyarabic acid. [6]

Finally, although the tool is very fast even for a very big nanoparticle, the algorithm could be improved to lower computational complexity and also fix bugs that might appear in the future.

ABBREVIATIONS - ACRONYMS

BRFAA	Biomedical Research Foundation of the Academy of Athens
CIF	Crystallographic Information File
CSS	Cascading Style Sheets
DFT	Density Functional Theory
DIT	Department of Informatics and Telecommunications
HTML	Hypertext Markup Language
ITMB	Information Technologies in Medicine and Biology
MATLAB	Matrix Laboratory
MC	Monte Carlo
MD	Molecular Dynamics
NP	Nanoparticle
NHRF	National Hellenic Research Foundation
NKUA	National and Kapodistrian University of Athens
PDB	Protein Data Bank file format
PHP	Hypertext Preprocessor
VESTA	Visualization for Electronic and Structural Analysis

ANNEX I

The manual of the website is the following:

A web based crystallographic tool for the construction of nanoparticles
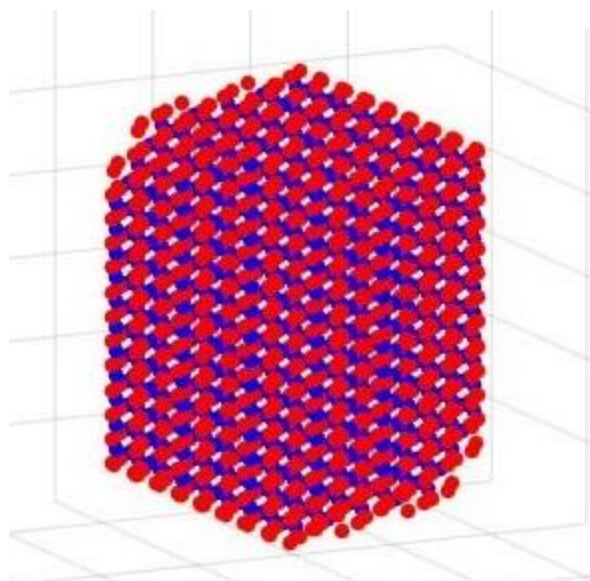
Alexios Chatzigoulas & Zoe Cournia

Biomedical Research Foundation

Academy of Athens

http://nanocrystal.vi-seem.eu/CrystalTool

Contents

1. Introduction

Nanoparticles are nano-engineered structures with size between 1-100 nm, with various, mainly industrial, applications such as in drug delivery systems [1], quantum computers, textiles (technical, medical, electrocontucting, anti-stain), industrial catalysts, food packaging and many others and are formed by crystals of materials. Individual crystals grow based on their crystal habits, which give the characteristic external shape of a crystal, but crystallographic files contain only the crystal structure and not its crystal shape. However, creating an initial starting conformation for modeling and simulation is tedious, because every crystalline material grows with a different crystal habit that determines its symmetry in nature. That gave us the motivation to provide an easily accessible web based crystallographic tool which can produce nanoparticles for simulation from any material as they grow in nature of any type, any size and any shape.

2. Methodology

In order to create nanoparticle models from any crystal structure guided by their preferred equilibrium shape in standard conditions (crystal habit), our algorithm uses input from quantum mechanical calculations based on the Wulff construction. The Wulff construction employs energy minimization arguments to demonstrate that certain crystal planes are preferred over others, with their distance from the origin being proportional to their surface energy [2]. The input parameters for determining this equilibrium nanoparticle structure are the preferred growing planes as Miller indices, the energy of each plane, and the desired size of the nanoparticle.

After inputting this data, the equilibrium shape is created with the following methodology. First, based on the crystallographic space group, the symmetric planes are produced based on the Miller indices, the fractional coordination system and the lattice parameters. In this procedure, we place the origin on the negative side of these planes and then we calculate the intersection points per three of the planes, discarding those that are on the positive side of at least one of the planes. Then, we obtain the faces of the equilibrium shape using the Quickhull algorithm on the remaining intersection points and the equilibrium shape is constructed by connecting these faces [3]. The unit cell of the crystal structure is produced from the asymmetric one (figure 1a), using again the lattice parameters and the symmetry operations of the crystallographic space group on the coordinates of the atoms. Finally, the supercell is constructed by replication of the unit cell across all three spatial directions (figure 1b) until the equilibrium shape is filled (figure 1c), and the coordinates are output to the user.
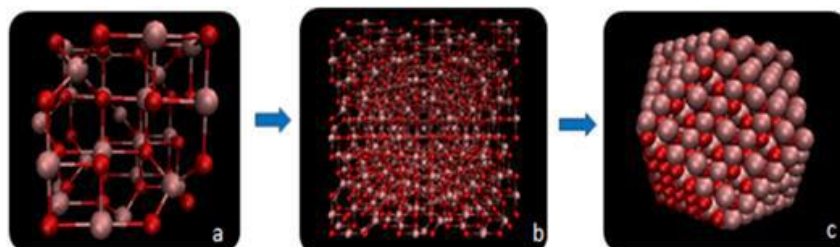
Figure 1. Given (a) an initial unit cell and (b) its replication in three dimensions, (c) the crystal habit of the nanoparticle can be reproduced in Cartesian coordinates using our algorithm given the Miller indices of the preferred growing planes, their energies and the desired nanoparticle size.

3. Description of the Program

This tool may be used to construct nanoparticles of any material given the crystal structure as input, the size of the nanoparticle, and the preferred growing planes and energies. It has been implemented as a web server using C++ and PHP and can be accessed at: http://nanocrystal.vi-seem.eu/CrystalTool..

1. Input

a. Crystal structure

The first input is the crystal structure given as a .cif file.

Select a .cif file: Choose File No file chosen

Choose Miller indices: **and the corresponding minimum surface energy:** remove

add new hkl triplet

Choose maximum radius of nanoparticle in: Å

Upload

For example we select the TiO2 rutile .cif file which can be downloaded from http://www.crystallography.net/cod/9009083.html [4].

Select a .cif file: Choose File TiO2_rutile.cif

Choose Miller indices: **and the corresponding minimum surface energy:** remove

add new hkl triplet

Choose maximum radius of nanoparticle in: Å

Upload

b. Miller indices and energies

The next inputs are the Miller indices and their corresponding minimum surface energies which can be found either from bibliography or from your own quantum mechanical calculations based on the Wulff construction. These energies can be in any units (but the same between them) because the Wulff construction results in a polyhedron that depends only on ratios between surface tensions and not on their absolute values.

There is an option to add many hkl triplets along with their minimum surface energies and to delete one in case that more are added.

In the TiO2 example the given Miller indices and their corresponding surface energies found in bibliography [5] are:

Miller indices	Energies
110	15.6
100	19.6
011	24.4
001	28.9

and inserted the following way:

c. Size of nanoparticle

The final input is the maximum radius of the nanoparticle in Angstroms which determines the size of the nanoparticle the user wants.

In our example let's choose 100 Angstroms.

A web based crystallographic tool for the construction of nanoparticles

Select a .cif file: Choose File   TiO2_rutile.cif

Choose Miller indices: 110   **and the corresponding minimum surface energy:** 15.6   remove
Choose Miller indices: 100   **and the corresponding minimum surface energy:** 19.6   remove
Choose Miller indices: 011   **and the corresponding minimum surface energy:** 24.4   remove
Choose Miller indices: 001   **and the corresponding minimum surface energy:** 28.9   remove

add new hkl triplet

Choose maximum radius of nanoparticle in: Å 100

Upload

After all these required inputs are fulfilled then hit the Upload button.

2. Output

As a result you have the choice to download the coordinates of the atoms in a .xyz file and a .pdb file.

Download .xyz file   Download .pdb file

Return

and to visualize the nanoparticle using the JSmol. In order to view the atoms in VDW right click on the nanoparticle → Style → Atoms → 100% VDW.
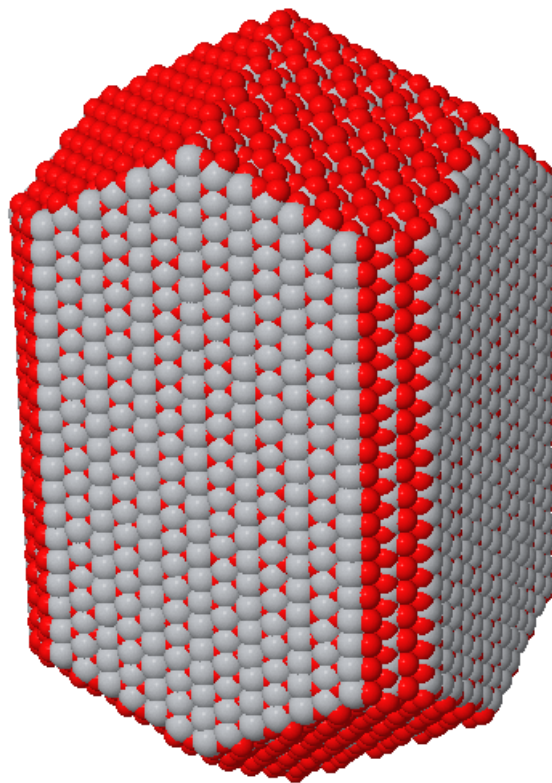
JSmol

Bibliography

[1] Patitsa, Maria, Konstantina Karathanou, Zoi Kanaki, Lamprini Tzioga, Natassa Pippa, Constantinos Demetzos, Dimitris A. Verganelakis, Zoe Cournia, and Apostolos Klinakis. "Magnetic nanoparticles coated with polyarabic acid demonstrate enhanced drug delivery and imaging properties for cancer theranostic applications." Scientific Reports 7 (2017).

[2] Barmparis, Georgios D., Zbigniew Lodziana, Nuria Lopez, and Ioannis N. Remediakis. "Nanoparticle shapes by using Wulff constructions and first-principles calculations." Beilstein journal of nanotechnology 6 (2015): 361.

[3] Barber, C. Bradford, David P. Dobkin, and Hannu Huhdanpaa. "The quickhull algorithm for convex hulls." ACM Transactions on Mathematical Software (TOMS) 22, no. 4 (1996): 469-483.

[4] Wyckoff, R. W. G. Crystal Structures Second edition. Interscience Publishers, New York, New York (1963): 239-444.

[5] Ramamoorthy, Madhavan, David Vanderbilt, and R. D. King-Smith. "First-principles calculations of the energetics of stoichiometric TiO 2 surfaces." Physical Review B 49.23 (1994): 16721.

REFERENCES

[1]   A. Keiper, "The nanotechnology revolution," *The New Atlantis,* no. 2, pp. 17-34, 2003.

[2]   R. P. Feynman, "There's plenty of room at the bottom," *Engineering and science,* vol. 23, no. 5, pp. 22-36, 1960.

[3]   N. Taniguchi, "On the basic concept of nano-technology," in *Proc. Intl. Conf. Prod. London, 1974*, 1974: British Society of Precision Engineering.

[4]   J. Demirdoven, "Nanotechnology Enabling BIM for Facility Owners," in *presentation in Ecobuild America 2012 conference, Washington, DC*, 2012.

[5]   Applications of nanoparticles. (n.d.). [image] Available at: https://prochimia.com/nanoparticles [Accessed 10 Dec. 2017].

[6]   M. Patitsa *et al.*, "Magnetic nanoparticles coated with polyarabic acid demonstrate enhanced drug delivery and imaging properties for cancer theranostic applications," *Scientific Reports,* vol. 7, no. 1, p. 775, 2017.

[7]   G. Lövestam *et al.*, "Considerations on a definition of nanomaterial for regulatory purposes," *Joint Research Centre (JRC) Reference Reports,* pp. 80004-1, 2010.

[8]   J. J. Brennan and K. M. Prewo, "Silicon carbide fibre reinforced glass-ceramic matrix composites exhibiting high strength and toughness," *Journal of Materials Science,* vol. 17, no. 8, pp. 2371-2383, 1982.

[9]   M. S. Lowry, D. R. Hubble, A. L. Wressell, M. S. Vratsanos, F. R. Pepe, and C. R. Hegedus, "Assessment of UV-permeability in nano-ZnO filled coatings via high throughput experimentation," *Journal of Coatings Technology and Research,* vol. 5, no. 2, pp. 233-239, 2008.

[10]   N. Nasongkla *et al.*, "Multifunctional polymeric micelles as cancer-targeted, MRI-ultrasensitive drug delivery systems," *Nano letters,* vol. 6, no. 11, pp. 2427-2430, 2006.

[11]   A. K. Gupta and M. Gupta, "Synthesis and surface engineering of iron oxide nanoparticles for biomedical applications," *Biomaterials,* vol. 26, no. 18, pp. 3995-4021, 2005.

[12]   S. H. Ng, J. Wang, D. Wexler, K. Konstantinov, Z. P. Guo, and H. K. Liu, "Highly Reversible Lithium Storage in Spheroidal Carbon-Coated Silicon Nanocomposites as Anodes for Lithium-Ion Batteries," *Angewandte Chemie International Edition,* vol. 45, no. 41, pp. 6896-6899, 2006.

[13]   D. Wang *et al.*, "Structurally ordered intermetallic platinum–cobalt core–shell nanoparticles with enhanced activity and stability as oxygen reduction electrocatalysts," *Nature materials,* vol. 12, no. 1, pp. 81-87, 2013.

[14]   C. Ostiguy, B. Roberge, and C. Woods, *Engineered Nanoparticles: Current Knowledge about OHS Risks and Prevention Measures*. Institut de recherche Robert-Sauvé en santé et en sécurité du travail, 2010.

[15]   Applications of nanoparticles. (n.d.). [image] Available at: https://prochimia.com/nanoparticles [Accessed 10 Dec. 2017].

[16]   R. Nagarajan, "Nanoparticles: building blocks for nanotechnology," ACS Publications, 2008.

[17]   Bose, A. (n.d.). Schematic diagram of various approaches for preparing nanoparticles. [image] Available at: http://www.pharmainfo.net/book/emerging-trends-nanotechnology-pharmacy-1introduction-nanotechnology/techniques-convert [Accessed 10 Dec. 2017].

[18]   T. S. Sreeprasad and T. Pradeep, "Noble metal nanoparticles," in *Springer Handbook of Nanomaterials*: Springer, 2013, pp. 303-388.

[19]   H. Fecht, E. Hellstern, Z. Fu, and W. Johnson, "Nanocrystalline metals prepared by high-energy ball milling," *Metallurgical and Materials Transactions A,* vol. 21, no. 9, pp. 2333-2337, 1990.

[20]   T. Sindhu, R. Sarathi, and S. R. Chakravarthy, "Understanding nanoparticle formation by a wire explosion process through experimental and modelling studies," *Nanotechnology,* vol. 19, no. 2, p. 025703, 2007.

[21]   A. Loiseau, F. Willaime, N. Demoncy, G. Hug, and H. Pascard, "Boron nitride nanotubes with reduced numbers of layers synthesized by arc discharge," *Physical Review Letters,* vol. 76, no. 25, p. 4737, 1996.

[22]   G. Nieman, J. Weertman, and R. Siegel, "Microhardness of nanocrystalline palladium and copper produced by inert-gas condensation," *Scripta Metallurgica,* vol. 23, no. 12, pp. 2013-2018, 1989.

[23]   A. M. Morales and C. M. Lieber, "A laser ablation method for the synthesis of crystalline semiconductor nanowires," *Science,* vol. 279, no. 5348, pp. 208-211, 1998.

[24]   S. Facsko *et al.*, "Formation of ordered nanoscale semiconductor dots by ion sputtering," *Science,* vol. 285, no. 5433, pp. 1551-1553, 1999.

[25]   S. Stankovich *et al.*, "Synthesis of graphene-based nanosheets via chemical reduction of exfoliated graphite oxide," *carbon,* vol. 45, no. 7, pp. 1558-1565, 2007.

[26]   Y.-Y. Yu, S.-S. Chang, C.-L. Lee, and C. C. Wang, "Gold nanorods: electrochemical synthesis and optical properties," *The Journal of Physical Chemistry B,* vol. 101, no. 34, pp. 6661-6664, 1997.

[27]   F. Kim, J. H. Song, and P. Yang, "Photochemical synthesis of gold nanorods," *Journal of the American Chemical Society,* vol. 124, no. 48, pp. 14316-14317, 2002.

[28]   J. H. Bang and K. S. Suslick, "Applications of ultrasound to the synthesis of nanostructured materials," *Advanced materials,* vol. 22, no. 10, pp. 1039-1059, 2010.

[29]   Y. Yang, S. Matsubara, L. Xiong, T. Hayakawa, and M. Nogami, "Solvothermal synthesis of multiple shapes of silver nanoparticles and their SERS properties," *The Journal of Physical Chemistry C,* vol. 111, no. 26, pp. 9095-9104, 2007.

[30]   T. Udaya Bhaskara Rao and T. Pradeep, "Luminescent Ag7 and Ag8 clusters by interfacial synthesis," *Angewandte Chemie International Edition,* vol. 49, no. 23, pp. 3925-3929, 2010.

[31]   D. Langevin, "Micelles and microemulsions," *Annual Review of Physical Chemistry,* vol. 43, no. 1, pp. 341-369, 1992.

[32]   T. Klaus, R. Joerger, E. Olsson, and C.-G. Granqvist, "Silver-based crystalline nanoparticles, microbially fabricated," *Proceedings of the National Academy of Sciences,* vol. 96, no. 24, pp. 13611-13614, 1999.

[33]   A. Pottier, C. Chanéac, E. Tronc, L. Mazerolles, and J.-P. Jolivet, "Synthesis of brookite TiO2 nanoparticles by thermolysis of TiCl4 in strongly acidic aqueous media," *Journal of Materials Chemistry,* vol. 11, no. 4, pp. 1116-1121, 2001.

[34]   J. O. Winter, N. Gomez, S. Gatzert, C. E. Schmidt, and B. A. Korgel, "Variation of cadmium sulfide nanoparticle size and photoluminescence intensity with altered aqueous synthesis conditions," *Colloids and Surfaces A: Physicochemical and Engineering Aspects,* vol. 254, no. 1, pp. 147-157, 2005.

[35]   S. Stoeva, K. J. Klabunde, C. M. Sorensen, and I. Dragieva, "Gram-scale synthesis of monodisperse gold colloids by the solvated metal atom dispersion method and digestive ripening and their organization into two-and three-dimensional structures," *Journal of the American Chemical Society,* vol. 124, no. 10, pp. 2305-2311, 2002.

[36]   S. Horikoshi and N. Serpone, "Introduction to nanoparticles," *Microwaves in Nanoparticle Synthesis: Fundamentals and Applications,* pp. 1-24, 2013.

[37]   J. Yu, M. L. Becker, and G. A. Carri, "A Molecular Dynamics Simulation of the Stability-Limited Growth Mechanism of Peptide-Mediated Gold-Nanoparticle Synthesis," *Small,* vol. 6, no. 20, pp. 2242-2245, 2010.

[38]   Q. Zeng, X. Jiang, A. Yu, and G. M. Lu, "Growth mechanisms of silver nanoparticles: a molecular dynamics study," *Nanotechnology,* vol. 18, no. 3, p. 035708, 2007.

[39]   B. Buesser, A. Grohn, and S. E. Pratsinis, "Sintering rate and mechanism of TiO2 nanoparticles by molecular dynamics," *The Journal of Physical Chemistry C,* vol. 115, no. 22, pp. 11030-11035, 2011.

[40]   B. Yang, M. Asta, O. Mryasov, T. Klemmer, and R. Chantrell, "Equilibrium Monte Carlo simulations of A1–L1 0 ordering in FePt nanoparticles," *Scripta Materialia,* vol. 53, no. 4, pp. 417-422, 2005.

[41]   O. Iglesias and A. Labarta, "Finite-size and surface effects in maghemite nanoparticles: Monte Carlo simulations," *Physical Review B,* vol. 63, no. 18, p. 184416, 2001.

[42]   A. Scullion, D. A. Thompson, and G. A. Botton, "Growth and kinetic Monte Carlo simulation of InAs quantum wires on vicinal substrates," *Journal of Crystal Growth,* vol. 412, pp. 87-94, 2015.

[43]   U. Riaz and S. Ashraf, "Computational Modeling of Nanoparticles," *Computational Nanotechnology: Modeling and Applications with MATLAB®,* p. 29, 2011.

[44]   G. Wulff, "Xxv. zur frage der geschwindigkeit des wachsthums und der auflösung der krystallflächen," *Zeitschrift für Kristallographie-Crystalline Materials,* vol. 34, no. 1-6, pp. 449-530, 1901.

[45]   G. Hadjisavvas, I. N. Remediakis, and P. C. Kelires, "Shape and faceting of Si nanocrystals embedded in a− Si O 2: A Monte Carlo study," *Physical Review B,* vol. 74, no. 16, p. 165419, 2006.

[46]   Y. Saito and T. Ueta, "Monte Carlo studies of equilibrium and growth shapes of a crystal," *Physical Review A,* vol. 40, no. 6, p. 3408, 1989.

[47]   G. D. Barmparis, A. E. Maniadaki, G. Kopidakis, and I. N. Remediakis, "Wulff construction and molecular dynamics simulations for Au nanoparticles," *J. Chem. Eng. Chem. Res,* 2016.

[48]   F. Baletto, C. Mottet, and R. Ferrando, "Molecular dynamics simulations of surface diffusion and growth on silver and gold clusters," *Surface Science,* vol. 446, no. 1, pp. 31-45, 2000.

[49]   Mathematical and Computational Modeling of Complex Molecular Systems (n.d.). Simulation methods in different length and time scales. [image] Available at: http://macomms.tem.uoc.gr/index.php/39-mmcaristeiaii/60-existing-knowledge-project-innovation-and-originality [Accessed 8 Jan. 2018].

[50]   M. A. Boles, D. Ling, T. Hyeon, and D. V. Talapin, "The surface science of nanocrystals," *Nature materials,* vol. 15, no. 2, pp. 141-153, 2016.

[51]   C. Rao, P. Thomas, and G. Kulkarni, "Basics of Nanocrystals," *Nanocrystals: Synthesis, Properties and Applications,* pp. 1-23, 2007.

[52]   P. P. Edwards, R. L. Johnston, and C. Rao, "On the Size-Induced Metal-Insulator Transition in Clusters and Small Particles," *Metal Clusters in Chemistry,* pp. 1454-1481, 1999.

[53]   C. Nützenadel, A. Züttel, D. Chartouni, G. Schmid, and L. Schlapbach, "Critical size and surface effect of the hydrogen interaction of palladium clusters," *The European Physical Journal D-Atomic, Molecular, Optical and Plasma Physics,* vol. 8, no. 2, pp. 245-250, 2000.

[54]   University of Cambridge (n.d.). The lattice parameters of the unit cell. [image] Available at: https://www.doitpoms.ac.uk/tlplib/crystallography3/parameters.php [Accessed 7 Nov. 2017].

[55]   C. Kittel, *Introduction to solid state physics*. Wiley, 2005.

[56]   Hoffmann, F. and Sartor, M. (n.d.). Crystal Structure = Lattice + Base/Motif. [image] Available at: https://crystalsymmetry.files.wordpress.com/2016/06/crystal_mooc_yt_en_01_09.pdf [Accessed 7 Nov. 2017].

[57]   E. N. Economou, *The Physics of Solids: Essentials and Beyond*. Springer Science & Business Media, 2010.

[58]   J. R. Hook and H. E. Hall, "Solid State Physics (The Manchester Physics Series)," ed: John Wiley and Sons Ltd, 1991.

[59]   The four centering types. (n.d.). [image] Available at: http://www.physics-in-a-nutshell.com/article/6/symmetry-crystal-systems-and-bravais-lattices [Accessed 8 Nov. 2017].

[60]   R. A. Evarestov, *Quantum chemistry of solids: LCAO treatment of crystals and nanostructures*. Springer Science & Business Media, 2013.

[61]   The four centering types. (n.d.). [image] Available at: http://www.physics-in-a-nutshell.com/article/6/symmetry-crystal-systems-and-bravais-lattices [Accessed 8 Nov. 2017].

[62]   S. H. Simon, *The Oxford solid state basics*. OUP Oxford, 2013.

[63]   The 14 Bravais lattices. (n.d.). [image] Available at: http://www.xtal.iqfr.csic.es/Cristalografia/parte_03_4-en.html [Accessed 8 Nov. 2017].

[64] E. W. Weisstein, "Crystallographic Point Groups," 2000.

[65] A. W. Jones, "Part II Group Theory," *Mathematics,* p. 157, 2017.

[66] H. Burzlaff and H. Zimmermann, "Point-group symbols," in *International Tables for Crystallography Volume A: Space-group symmetry*: Springer, 2006, pp. 818-820.

[67] B. Kojić-Prodić and Z. Štefanić, "Symmetry versus asymmetry in the molecules of life: homomeric protein assemblies," *Symmetry,* vol. 2, no. 2, pp. 884-906, 2010.

[68] Crystallographic point groups. (n.d.). [image] Available at: https://en.wikipedia.org/wiki/Crystallographic_point_group [Accessed 9 Nov. 2017].

[69] H. Hiller, "Crystallography and cohomology of groups," *The American Mathematical Monthly,* vol. 93, no. 10, pp. 765-779, 1986.

[70] Martínez-Ripoll, M. (n.d.). The symmetry of crystals. [image] Available at: http://www.xtal.iqfr.csic.es/Cristalografia/parte_03-en.html [Accessed 5 Feb. 2018].

[71] Ong, S. (2016). Sequensce of symmetry operations. [image] Available at: https://image.slidesharecdn.com/04-symmetryincrystallography-160329175434/95/ucsd-nano106-04-symmetry-in-crystallography-21-638.jpg?cb=1459274124 [Accessed and edited 6 Feb. 2018].

[72] Symbols for the 230 space groups. (n.d.). [image] Available at: http://atom.uwaterloo.ca/CHEM/750/Lectures%202007/SSNT-3-Surface%20Structure%20I.htm [Accessed 9 Nov. 2017].

[73] R. J. Tilley, *Understanding solids: the science of materials*. John Wiley & Sons, 2004.

[74] Nelson, S. (2016). Miller Indices. [image] Available at: http://www.tulane.edu/~sanelson/eens211/axial_ratios_paramaters_miller_indices.htm [Accessed 9 Nov. 2017].

[75] School of Biological & Chemical Sciences at Queen Mary, University of London (n.d.). Miller Indices (hkl). [image] Available at: http://www.chem.qmul.ac.uk/surfaces/scc/scat1_1b.htm [Accessed 9 Nov. 2017].

[76] Unit cell definition using parallelepiped with lengths a, b, c and angles between the sides given by α, β, γ. (2016). [image] Available at: https://ipfs.io/ipfs/QmXoypizjW3WknFiJnKLwHCnL72vedxjQkDDP1mXWo6uco/wiki/Fractional_coordinates.html [Accessed 14 Nov. 2017].

[77] G. Wulff, "Some Theorems Concerning the Growth and Dissolution Rates of Crystals," *Ger.), Z. Kristallogr,* vol. 34, no. 5, pp. 449-530, 1901.

[78] J. W. Gibbs, "On the equilibrium of heterogeneous substances," *American Journal of Science,* no. 96, pp. 441-458, 1878.

[79] G. D. Barmparis, Z. Lodziana, N. Lopez, and I. N. Remediakis, "Nanoparticle shapes by using Wulff constructions and first-principles calculations," *Beilstein journal of nanotechnology,* vol. 6, p. 361, 2015.

[80] Y.-C. Zou *et al.*, "Surface-energy engineered Bi-doped SnTe nanoribbons with weak antilocalization effect and linear magnetoresistance," *Nanoscale,* vol. 8, no. 46, pp. 19383-19389, 2016.

[81] X.-Y. Liu and P. Bennema, "Theoretical consideration of the growth morphology of crystals," *Physical Review B,* vol. 53, no. 5, p. 2314, 1996.

[82] K. Momma and F. Izumi, "VESTA: a three-dimensional visualization system for electronic and structural analysis," *Journal of Applied Crystallography,* vol. 41, no. 3, pp. 653-658, 2008.

[83] K. Momma and F. Izumi, "VESTA 3 for three-dimensional visualization of crystal, volumetric and morphology data," *Journal of Applied Crystallography,* vol. 44, no. 6, pp. 1272-1276, 2011.

[84] C. F. Macrae *et al.*, "Mercury CSD 2.0–new features for the visualization and investigation of crystal structures," *Journal of Applied Crystallography,* vol. 41, no. 2, pp. 466-470, 2008.

[85] C. F. Macrae *et al.*, "Mercury: visualization and analysis of crystal structures," *Journal of Applied Crystallography,* vol. 39, no. 3, pp. 453-457, 2006.

[86]   I. J. Bruno *et al.*, "New software for searching the Cambridge Structural Database and visualizing crystal structures," *Acta Crystallographica Section B: Structural Science,* vol. 58, no. 3, pp. 389-397, 2002.

[87]   R. Taylor and C. F. Macrae, "Rules governing the crystal packing of mono-and dialcohols," *Acta Crystallographica Section B: Structural Science,* vol. 57, no. 6, pp. 815-827, 2001.

[88]   W. Kaminsky, "WinXMorph: a computer program to draw crystal morphology, growth sectors and cross sections with export files in VRML V2. 0 utf8-virtual reality format," *Journal of applied crystallography,* vol. 38, no. 3, pp. 566-567, 2005.

[89]   W. Kaminsky, "From CIF to virtual morphology using the WinXMorph program," *Journal of Applied Crystallography,* vol. 40, no. 2, pp. 382-385, 2007.

[90]   D. S. Biovia, "Materials Studio Modeling Environment," *Dassault Systèmes, San Diego,* 2015.

[91]   J. Rakovan, "Computer Programs for Drawing Crystal Shapes and Atomic Structures," *Rocks & Minerals,* vol. 93, no. 1, pp. 60-64, 2018.

[92]   M. O. Toolbox, "The MathWorks Inc," *Natick, MA,* 2002.

[93]   B. Stroustrup, *The C++ programming language.* Pearson Education India, 2000.

[94]   G. Schlossnagle, *Advanced PHP programming: a practical guide to developing large-scale web sites and applications with PHP 5.* Pearson Education, 2004.

[95]   M. G. Rossmann and D. M. Blow, "The detection of sub-units within the crystallographic asymmetric unit," *Acta Crystallographica,* vol. 15, no. 1, pp. 24-31, 1962.

[96]   Calculate the plane equation given three points. (n.d.). [image] Available at: http://keisan.casio.com/has10/SpecExec.cgi?id=system/2006/1223596129 [Accessed 14 Nov. 2017].

[97]   Sunday, D. (2012). Intersections of planes. [image] Available at: http://geomalgorithms.com/a05-_intersect-1.html [Accessed and edited 14 Nov. 2017].

[98]   Dawkins, P. (n.d.). The 3-D Coordinate System. [image] Available at: http://geomalgorithms.com/a05-_intersect-1.html [Accessed and edited 14 Nov. 2017].

[99]   C. B. Barber, D. P. Dobkin, and H. Huhdanpaa, "The quickhull algorithm for convex hulls," *ACM Transactions on Mathematical Software (TOMS),* vol. 22, no. 4, pp. 469-483, 1996.

[100]   3D convex hull of 120 point cloud. (2015). [image] Available at: https://en.wikipedia.org/wiki/Convex_hull [Accessed 15 Nov. 2017].

[101]   Gregorius, D. (2014). Implementing QuickHull. [image] Available at: http://media.steampowered.com/apps/valve/2014/DirkGregorius_ImplementingQuickHull.pdf [Accessed and edited 15 Nov. 2017].

[102]   M. Nespolo, "International Tables for Crystallography, Volume A, Space-group symmetry. Edited by Mois I. Aroyo. Wiley, 2016. Pp. xxi+ 873. Price GBP 295.00, EUR 354.00 (hardcover). ISBN 978-0-470-97423-0," *Acta Crystallographica Section A: Foundations and Advances,* vol. 73, no. 3, 2017.

[103]   S. R. Hall, F. H. Allen, and I. D. Brown, "The crystallographic information file (CIF): a new standard archive file for crystallography," *Acta Crystallographica Section A: Foundations of Crystallography,* vol. 47, no. 6, pp. 655-685, 1991.

[104]   A. Merkys, A. Vaitkus, J. Butkus, M. Okulič-Kazarinas, V. Kairys, and S. Gražulis, "COD:: CIF:: Parser: an error-correcting CIF parser for the Perl language," *Journal of applied crystallography,* vol. 49, no. 1, pp. 292-301, 2016.

[105]   S. Gražulis, A. Merkys, A. Vaitkus, and M. Okulič-Kazarinas, "Computing stoichiometric molecular composition from crystal structures," *Journal of applied crystallography,* vol. 48, no. 1, pp. 85-91, 2015.

[106]   S. Gražulis *et al.*, "Crystallography Open Database (COD): an open-access collection of crystal structures and platform for world-wide collaboration," *Nucleic acids research,* vol. 40, no. D1, pp. D420-D427, 2011.

[107]   S. Gražulis *et al.*, "Crystallography Open Database–an open-access collection of crystal structures," *Journal of Applied Crystallography,* vol. 42, no. 4, pp. 726-729, 2009.

[108]   R. T. Downs and M. Hall-Wallace, "The American Mineralogist crystal structure database," *American Mineralogist,* vol. 88, no. 1, pp. 247-250, 2003.

[109]   T. Berners-Lee and D. Connolly, "Hypertext markup language (html)," *CERN, Geneva, Switzerland,* vol. 13, 1993.

[110]   H. W. Lie and B. Bos, *Cascading style sheets: Designing for the web.* Addison-Wesley Professional, 2005.

[111]   C. Severance, "Javascript: Designing a language in 10 days," *Computer,* vol. 45, no. 2, pp. 7-8, 2012.

[112]   R. M. Hanson, "Jmol–a paradigm shift in crystallographic visualization," *Journal of Applied Crystallography,* vol. 43, no. 5, pp. 1250-1260, 2010.

[113]   R. M. Hanson, J. Prilusky, Z. Renjian, T. Nakane, and J. L. Sussman, "JSmol and the Next-Generation Web-Based Representation of 3D Molecular Structure as Applied to Proteopedia," *Israel Journal of Chemistry,* vol. 53, no. 3-4, pp. 207-216, 2013.

[114]   G. D. Gatta, I. Kantor, T. B. Ballaran, L. Dubrovinsky, and C. McCammon, "Effect of non-hydrostatic conditions on the elastic behaviour of magnetite: an in situ single-crystal X-ray diffraction study," *Physics and Chemistry of Minerals,* vol. 34, no. 9, pp. 627-635, 2007.

[115]   D. Santos-Carballal, A. Roldan, R. Grau-Crespo, and N. H. de Leeuw, "A DFT study of the structures, stabilities and redox behaviour of the major surfaces of magnetite Fe 3 O 4," *Physical Chemistry Chemical Physics,* vol. 16, no. 39, pp. 21082-21097, 2014.

[116]   R. W. Wyckoff, "Crystal Structures, 1963, vol. 1," *Search PubMed,* pp. 239-444.

[117]   M. Ramamoorthy, D. Vanderbilt, and R. King-Smith, "First-principles calculations of the energetics of stoichiometric TiO 2 surfaces," *Physical Review B,* vol. 49, no. 23, p. 16721, 1994.

[118]   Y. Janssen *et al.*, "Reciprocal salt flux growth of LiFePO4 single crystals with controlled defect concentrations," *Chemistry of Materials,* vol. 25, no. 22, pp. 4574-4584, 2013.

[119]   L. Wang, F. Zhou, Y. Meng, and G. Ceder, "First-principles study of surface properties of Li Fe P O 4: Surface energy, structure, Wulff shape, and surface redox potential," *Physical Review B,* vol. 76, no. 16, p. 165435, 2007.

[120]   M. Singh, "First principle study of crystal growth morphology: An application to crystalline urea," *arXiv preprint cond-mat/0602385,* 2006.

[121]   J. D. H. Donnay and D. Harker, "A new law of crystal morphology extending the law of Bravais," *Am. Mineral,* vol. 22, no. 5, pp. 446-467, 1937.

[122]   P. Hartman and W. Perdok, "On the relations between structure and morphology of crystals. I," *Acta Crystallographica,* vol. 8, no. 1, pp. 49-52, 1955.

[123]   P. Hartman and W. Perdok, "On the relations between structure and morphology of crystals. II," *Acta Crystallographica,* vol. 8, no. 9, pp. 521-524, 1955.

[124]   P. Hartman and W. Perdok, "On the relations between structure and morphology of crystals. III," *Acta Crystallographica,* vol. 8, no. 9, pp. 525-529, 1955.

[125]   J. Rijpkema, H. Knops, P. Bennema, and J. Van der Eerden, "Determination of the Ising critical temperature of F slices with an application to garnet," *Journal of Crystal Growth,* vol. 61, no. 2, pp. 295-306, 1983.

[126]   R. Docherty, G. Clydesdale, K. Roberts, and P. Bennema, "Application of Bravais-Friedel-Donnay-Harker, attachment energy and Ising models to predicting and understanding the morphology of molecular crystals," *Journal of Physics D: Applied Physics,* vol. 24, no. 2, p. 89, 1991.